The role of radiologic imaging in the diagnosis of adrenal tumors: a literature review

Ruta Pupalyte[1], Algidas Basevicius[2]

[1]*Faculty of Medicine, Lithuanian University of Health Sciences, Kaunas, Lithuania*
[2]*Department of Radiology, Lithuanian University of Health Sciences, Kaunas, Lithuania*

ABSTRACT

Background and aim. The adrenal tumors are a reasonably common pathology. Radiologic imaging detects an adrenal neoplasm in approximately 4% of the patients incidentally. It is also a valuable tool that assists in determining a diagnosis. Furthermore, it may facilitate the further investigation and management of the lesion. This article aims to assess imaging features that are characteristic of the most common adrenal tumors.

Materials and methods. A selective search was carried out for relevant studies concerning radiologic imaging of adrenal adenoma, myelolipoma, pheochromocytoma, carcinoma, metastases, neural crest tumors, lymphoma, hemangioma, lymphangioma, and schwannoma. Medline (PubMed), Cochrane Library, SpringerLink and ScienceDirect databases were used.

Results. US is helpful for the screening of masses in the suprarenal region. Nevertheless, its findings have to be verified by CT or MRI. The golden standard of assessing adrenal tumors is native CT. Those lesions which present with probable malignant features should be evaluated using dynamic contrast-enhanced CT. Chemical shift MRI is a feasible alternative, especially in lipomatous masses. PET/CT is recommended for patients with large or indeterminate lesions.

Conclusion. Adrenal CT protocol is the most reliable technique in the differentiation of these diverse neoplasms. On the other hand, CS-MRI is indispensable for verifying intratumoral adipose tissue and, consequently, selecting the most appropriate approach to manage the mass. Furthermore, PET/CT permits characterizing indistinctive tumors and their potential metastatic spread.

Keywords: adrenal adenoma, pheochromocytoma, adrenocortical carcinoma, adrenal metastasis, computed tomography, magnetic resonance imaging

INTRODUCTION

The adrenal tumors are a reasonably common pathology. Clinical manifestations of these lesions are various; they cause abdominal pain, distention or fever [1]. However, the majority of the masses are asymptomatic. Although they originate from hormone-secreting cells in the adrenal cortex or medulla, the tumors are usually non-functional [2]. Hence, an adrenal mass often is a coincidental imaging finding. Adrenal tumors are found incidentally in approximately 4% of the patients during an abdominal CT scan due to unrelated symptoms [3].

Initial clinical workup, including examination of the patient and laboratory tests, is used in distinguishing the probable type of the tumor. Radiologic imaging is also a valuable tool that assists in determining an accurate diagnosis. Consequently, precise evaluation of imaging findings allows reducing the number of adrenal biopsies, surgeries and complications [4]. Therefore, the knowledge of imaging techniques and features associated with a particular pathology is immensely beneficial.

AIM

To evaluate radiologic imaging features that are representative of the most common adrenal tumors.

MATERIALS AND METHODS

A selective search was carried out for relevant studies concerning radiologic imaging of adenoma, myelolipoma, pheochromocytoma, carcinoma, metastases, neural crest tumors, lymphoma, hemangioma, lymphangioma, and schwannoma of the adrenal gland. We chose databases from the subscription list of Lithuanian University of

Health Sciences. Medline (PubMed), Cochrane Library, SpringerLink and ScienceDirect databases were used.

RESULTS

Adrenal lesions might not accurately visualize on conventional ultrasound (US) due to small size, stomach or intestinal gas, obesity or severe liver steatosis. US is helpful for the screening of masses in the suprarenal region. Nevertheless, its findings have to be verified by computed tomography (CT) or magnetic resonance imaging (MRI).

The golden standard of assessing adrenal tumors is CT [5]. Smaller, slow-growth lesions are presumably benign [6, 7]. Moreover, the attenuation value of 10 Hounsfield units (HU) or less suggests a benign mass on native CT [8–10]. If unenhanced CT scan displays feature associated with malignancy, dynamic contrast-enhanced CT (DCE-CT) with 15-min delayed acquisition through the upper abdomen should be performed [11].

Neoplasms of the adrenal gland have a distinctive pattern of the contrast washout [12]. Moreover, quantitative parameters, such as total percentage washout (APW) and relative percentage washout (RPW), can be calculated [13]. This radiologic framework allows differentiating the lesions more precisely.

Adrenal tumors should also be evaluated using chemical shift MRI (CS-MRI) [14]. The sequence

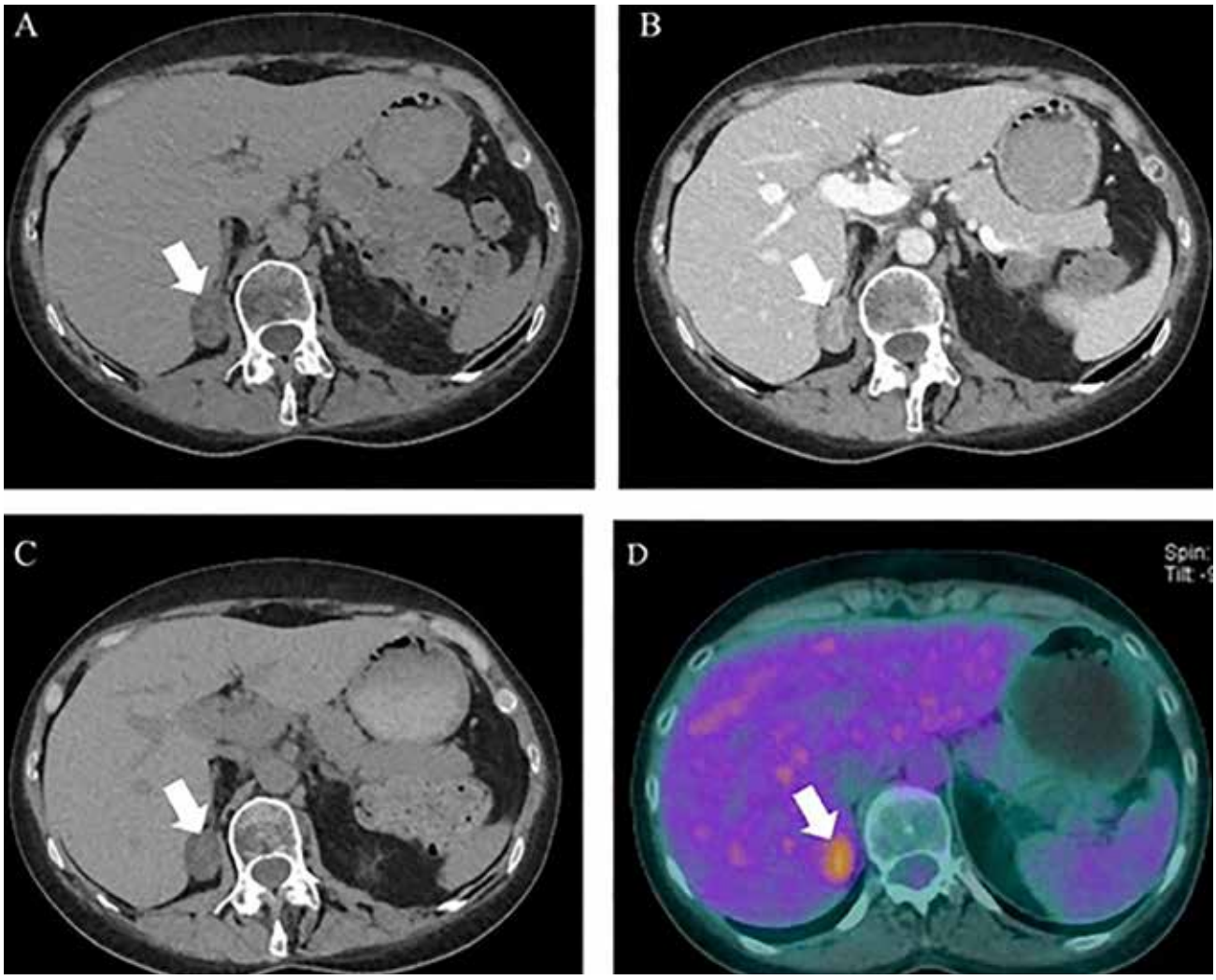

Figure 1. Axial unenhanced CT (A), DCE-CT during the portal venous phase (B) and 15-min delayed CT scans demonstrate well-defined hypoattenuated adrenal lesion (arrow) with early enhancement and rapid washout. SUVmax of the mass is 4.1 on 18F-FDG PET/CT (D). Imaging findings are suggestive of adrenal adenoma. (Humbert, AL, Lecoanet G, Moog S, Bouderraoui F, Bresler L, Vignaud JM, Chevalier E, Brunaud L, Klein M, Cuny T. The computed tomography adrenal wash-out analysis properly classifies cortisol secreting adrenocortical adenomas. Endocrine 2018; 59: 529-537)

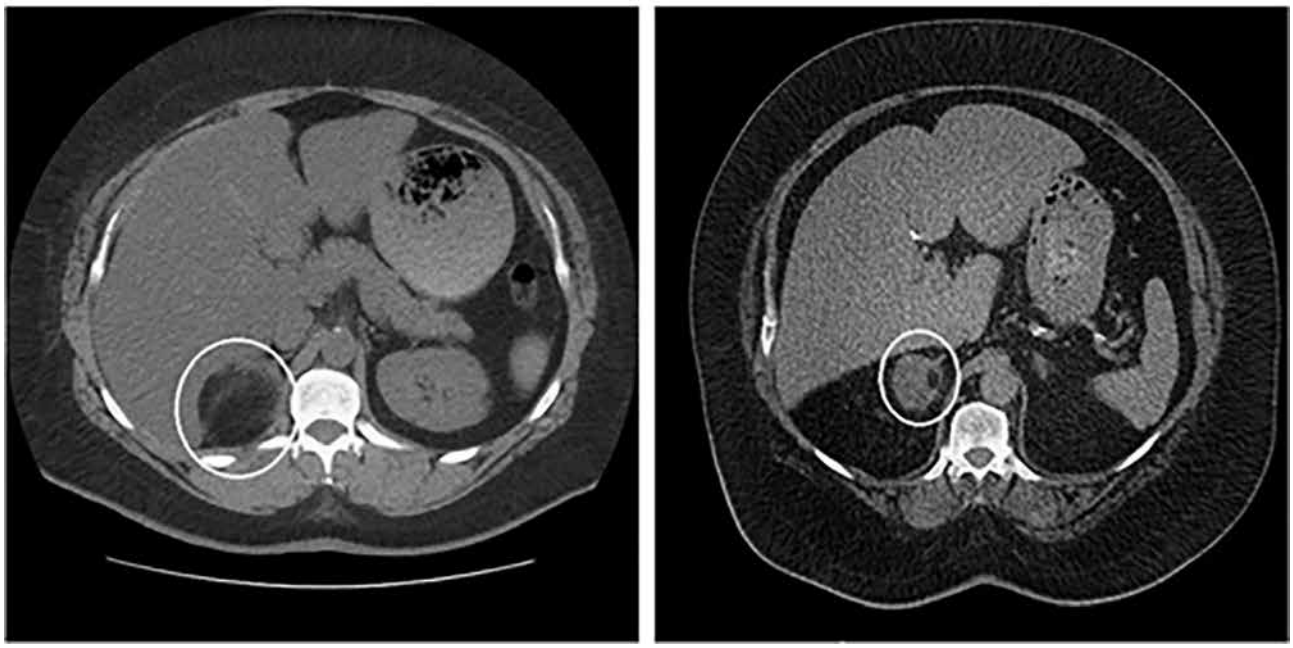

Figure 2. Myelolipoma of almost 100% macroscopic fat (circle) is observed in the right adrenal gland on axial unenhanced CT (A). Its attenuation value is lower than of myelolipoma containing approximately 10% macroscopic fat (B). (Campbell MJ, Obasi M, Wu B, Corwin MT, Fananapazir G. The radiographically diagnosed adrenal myelolipoma: what do we really know? Endocrine 2017; 58: 289-294)

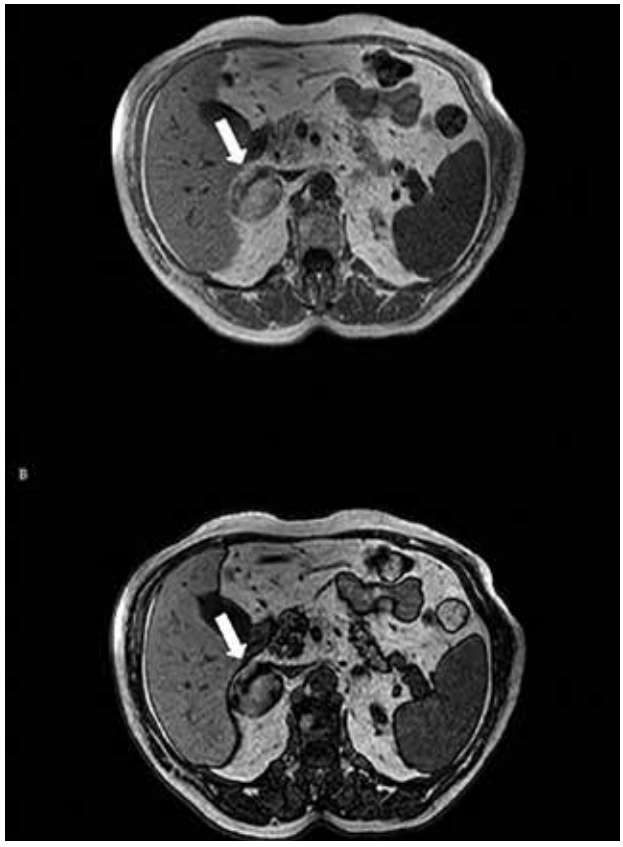

Figure 3. A loss of SI is displayed within adrenal myelolipoma (arrow) between the in-phase (A) and opposed-phase (B) axial CS-MRI. (Lesbats-Jacquot V, Cucchi JM, Amoretti N, Novellas S, Chevallier P, Bruneton JN. Lipomatous tumors of the adrenals – a report on 18 cases and review of the literature. Clin Imag 2007; 31: 335-339)

determines a loss of signal intensity (SI) on opposed-phase images compared to in-phase images. This signal drop correlates to intracytoplasmic fat and leads to a presumption of a benign mass [15]. CS-MRI is superior to DCE-CT only in those cases where the unenhanced attenuation value of the adrenal lesion is < 80 HU [16]. If a hyperattenuating tumor presents, DCE-CT achieves higher sensitivity than CS-MRI [17]. However, MRI is appropriate in pregnant patients or those with iodine hypersensitivity and reduced renal function.

Diffusion-weighted MRI (DW-MRI) is not routinely used for separating adrenal neoplasms [18].

Nuclear medicine, especially positron emission tomography (PET), plays a role in the differential diagnosis of adrenal tumors. Various radioisotopes are used, the most common one being fluorine-18-fludeoxyglucose (18F-FDG). A hybrid technique, PET/CT, is recommended for patients with large or indeterminate lesions. Increased metabolic activity of 18F-FDG is characteristic of malignant masses [8, 9, 19–22]. Even though PET/CT demonstrates high accuracy, it is still inferior to DCE-CT [23].

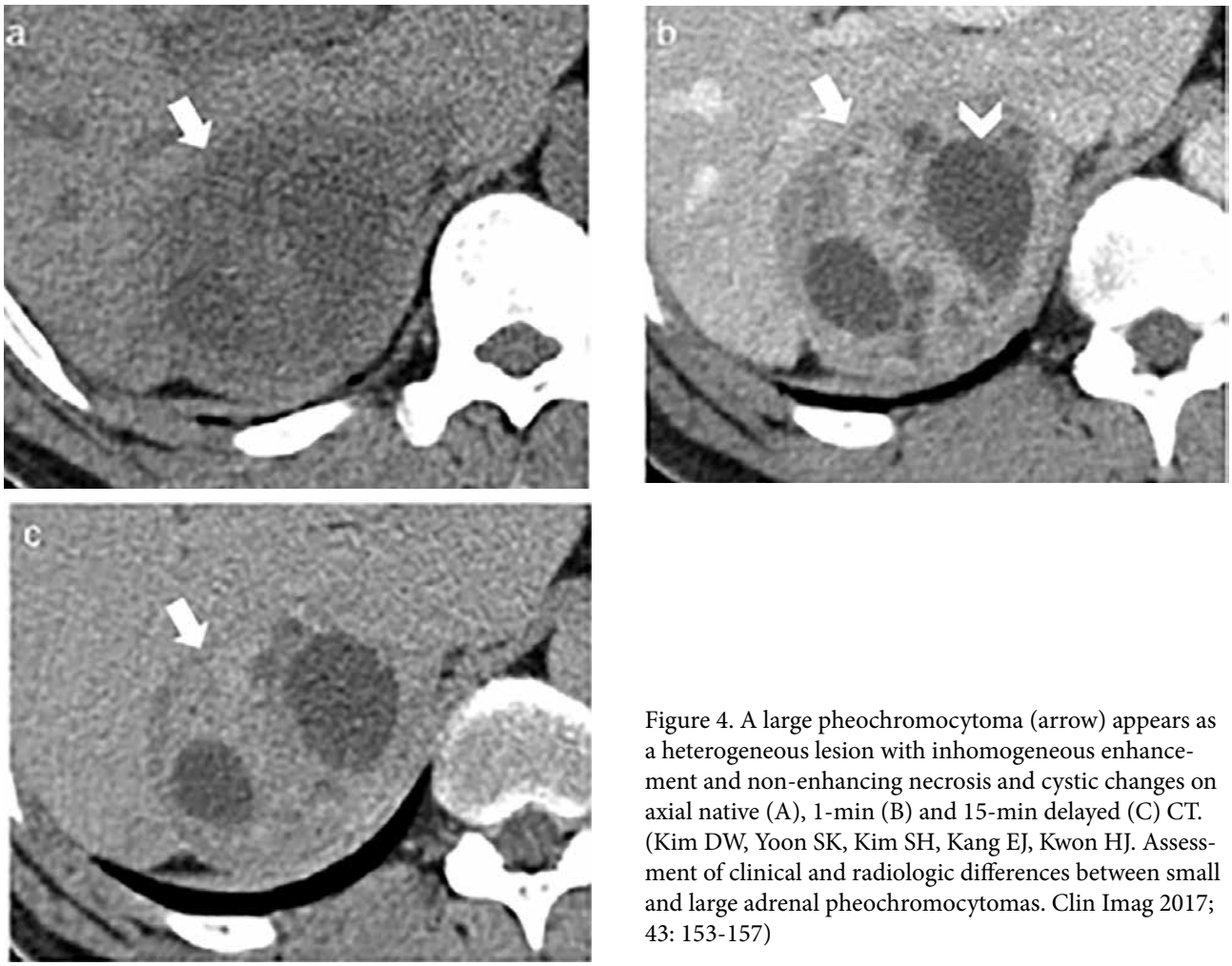

Figure 4. A large pheochromocytoma (arrow) appears as a heterogeneous lesion with inhomogeneous enhancement and non-enhancing necrosis and cystic changes on axial native (A), 1-min (B) and 15-min delayed (C) CT. (Kim DW, Yoon SK, Kim SH, Kang EJ, Kwon HJ. Assessment of clinical and radiologic differences between small and large adrenal pheochromocytomas. Clin Imag 2017; 43: 153-157)

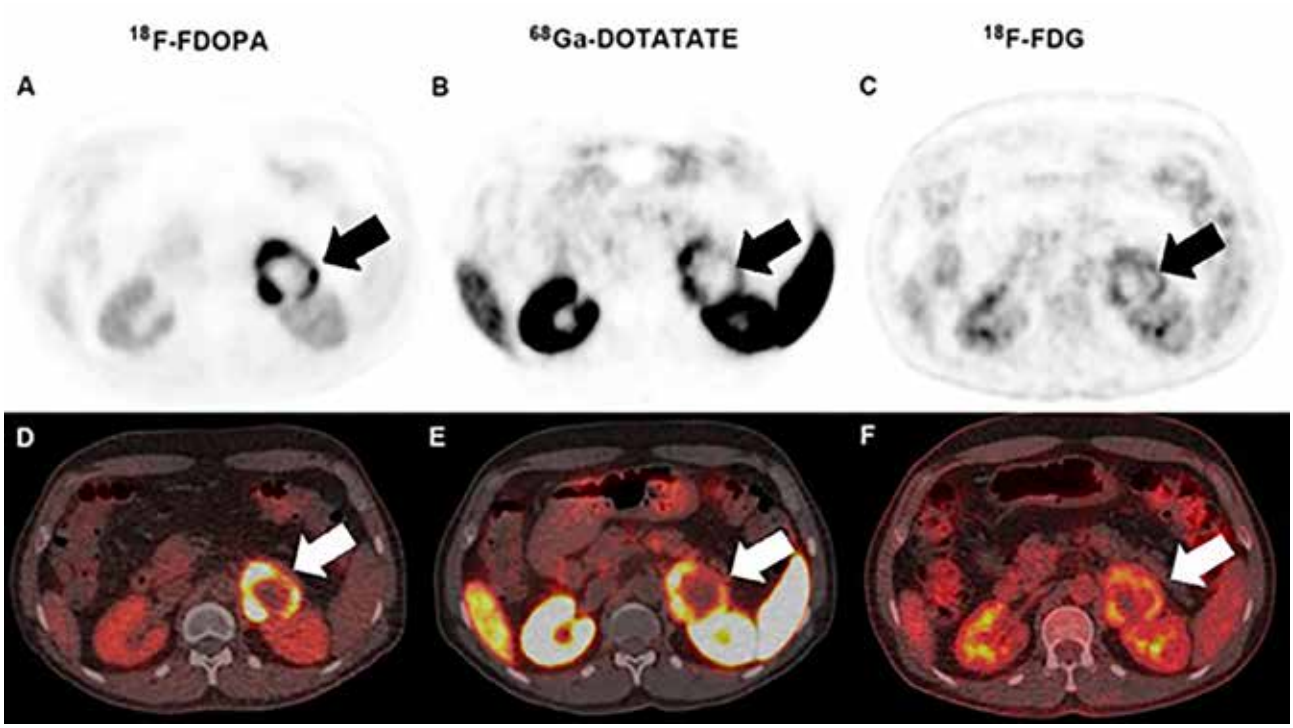

Figure 5. An avid peripheral uptake of radioisotopes with central photopenia (arrow) is depicted in the left adrenal gland on axial attenuation-corrected 18F-FDOPA, 68Ga-DOTATATE, 18F-FDG PET (A-C) and PET/CT (D-F) images. These features imply the presence of pheochromocytoma. (Taieb D, Jha A, Guerin C, Pang Y, Adams KT, Chen CC, Romanet P, Roche P, Essamet W, Ling A et al. 18F-FDOPA PET/CT imaging of MAX-related pheochromocytoma. J Clin Endocrinol Metab 2018; 103(4): 1574-1582)

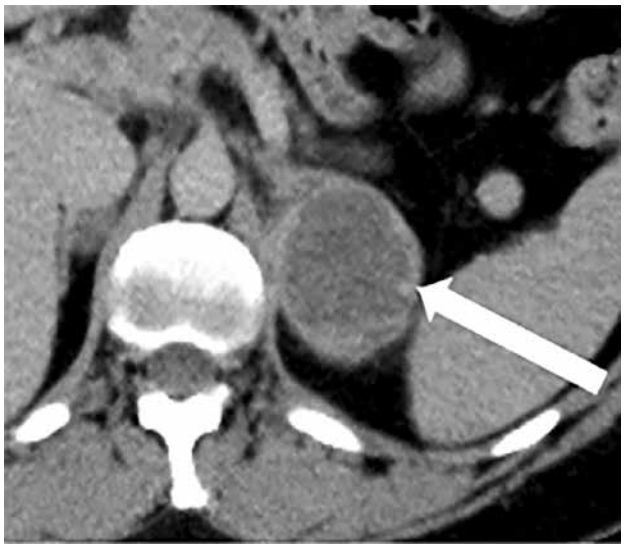

Figure 6. Adrenocortical carcinoma (arrow) presents with a large central non-enhancing hypodense region consistent with necrosis on axial native CT. (Thomas AJ, Habra MA, Bhosale PR, Qayyum AA, Ahmed K, Vicens R, Elsayes KM. Interobserver agreement in distinguishing large adrenal adenomas and adrenocortical carcinomas on computed tomography. Abdom Radiol 2018; 43: 3101-3108)

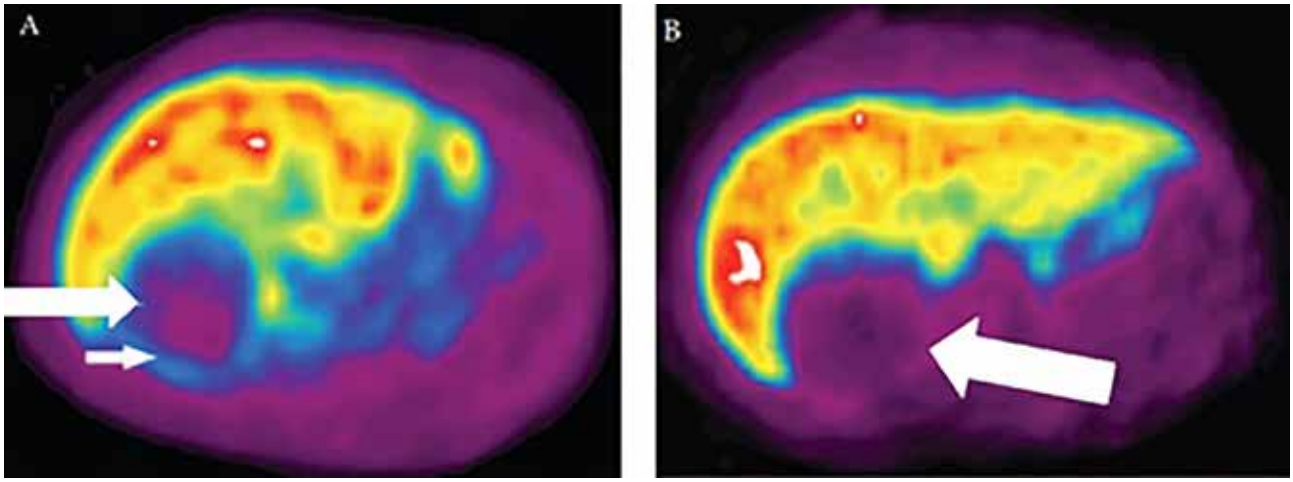

Figure 7. A lack of 11C-MTO uptake within a necrotic adrenal carcinoma (long arrow) is assessed on PET (A). However, a reminiscent uptake (short arrow) can be seen. On the other hand, pheochromocytoma (arrow) does not take up 11C-MTO at any rate (B). (Hennings J, Lindhe O, Bergstrom M, Langstrom B, Sundin A, Hellman P. [11C] Metomidate positron emission tomography of adrenocortical tumors in correlation with histopathological findings. J Clin Endocrinol Metab 2006; 91(4):1410-1414)

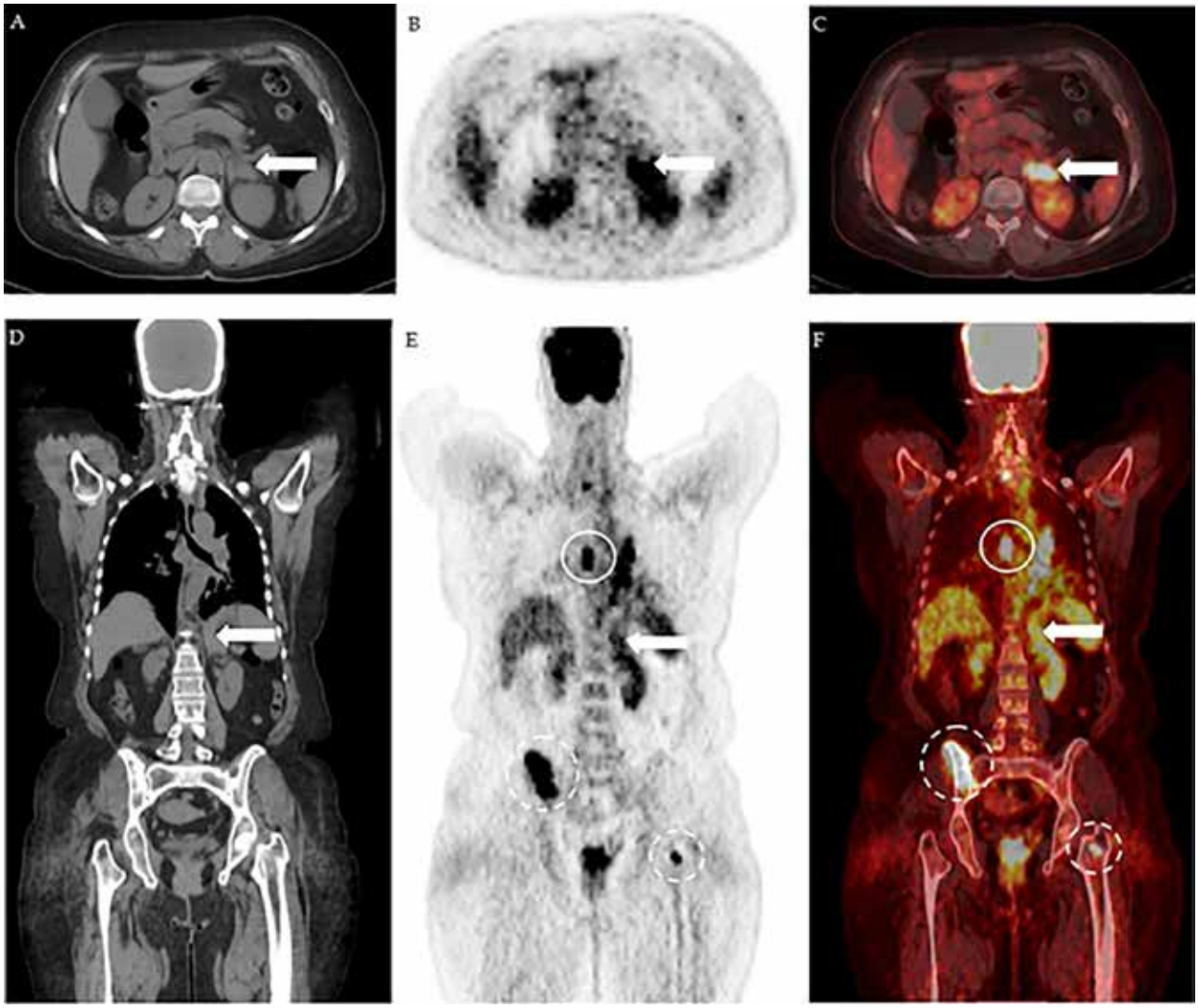

Figure 8. Adrenal metastasis is depicted on axial unenhanced CT (A), attenuation-corrected 18F-FDG PET (B) and fused PET/CT images (C). CT displays a well-circumscribed left adrenal tumor (arrow); increased 18F-FDG uptake is observed on PET and PET/CT. The primary lung cancer (continuous circle) and metastatic bone lesions (dashed circle) are seen on coronal plane of these images (D-F). (Refaat R, Elghazaly H. Employing 18F-FDG PET/CT for distinguishing benign from metastatic adrenal masses. Egypt J Radiol Nucl Med 2017; 48: 1065-1071)

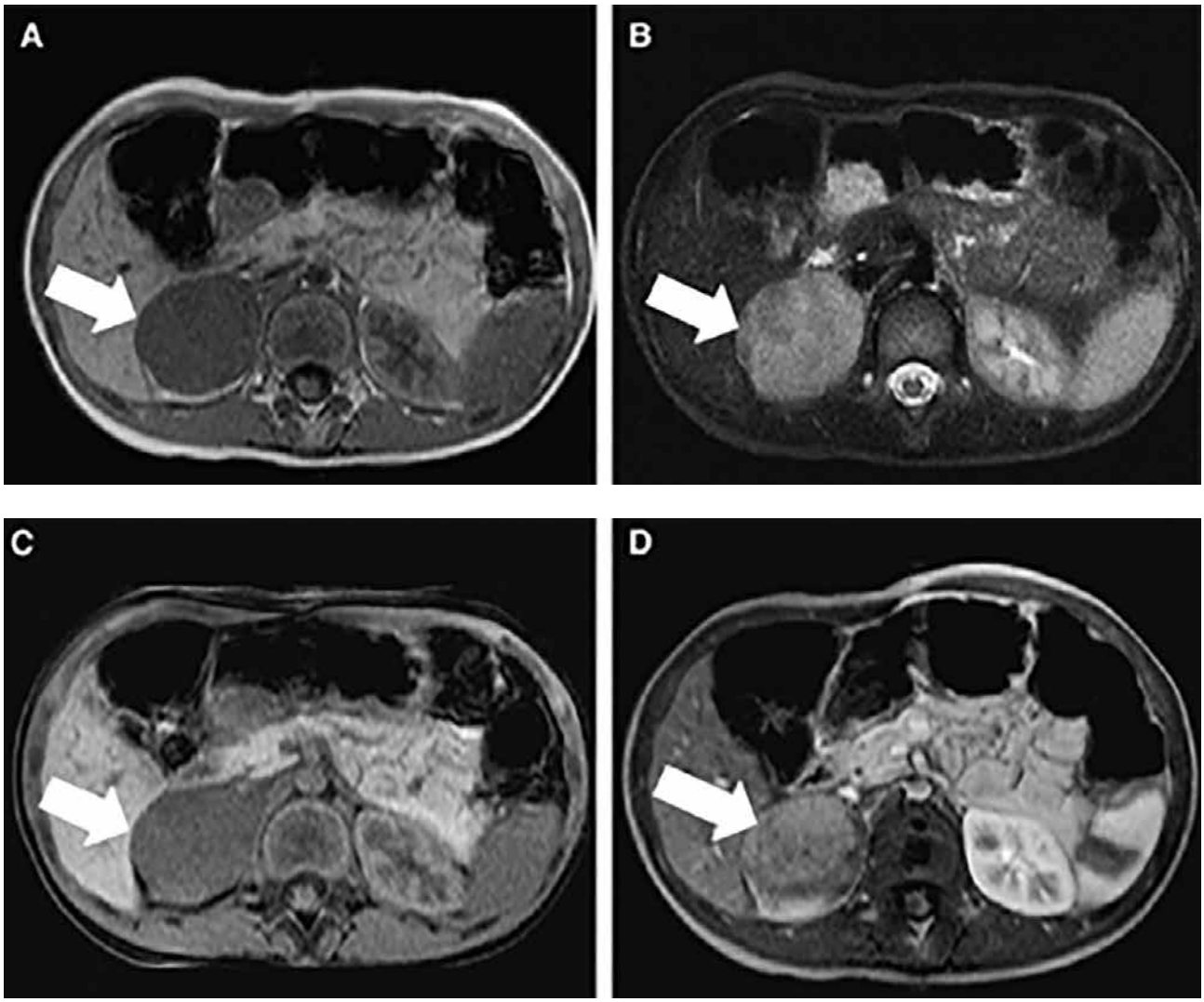

Figure 9. Ganglioneuroma (arrow) of the right adrenal gland is demonstrated as homogeneous and hypointense on MRI T1W image (A), heterogeneous and hyperintense on T2W image (B), homogeneous and isointense on fat-supressed T1W image (C). After administration of the contrast agent, a slight and heterogeenous enhancement is observed (D). (Qing Y, Bin X, Jian W, Li G, Linhui W, Bing L, Huiqing W, Inghao S. Adrenal ganglioneuromas: a 10-year experience in a Chinese population. Surgery 2010; 147(6): 854-860)

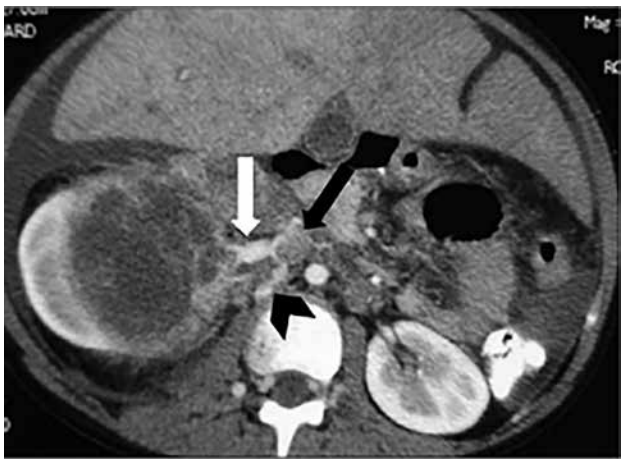

Figure 10. A heterogeneous hypoattenuated mass (white arrow), seen on axial contrast-enhanced CT, suggests a neuroblastoma. Thrombosis of the inferior vena cava (black arrow) is also displayed. It drains into a collateral vein (arrowhead). (Mehta SV, Lim-Dunham JE. Ultrasonographic appearance of pediatric abdominal neuroblastoma with inferior vena cava extension. J Ultrasound Med 2003; 22: 1091-1095)

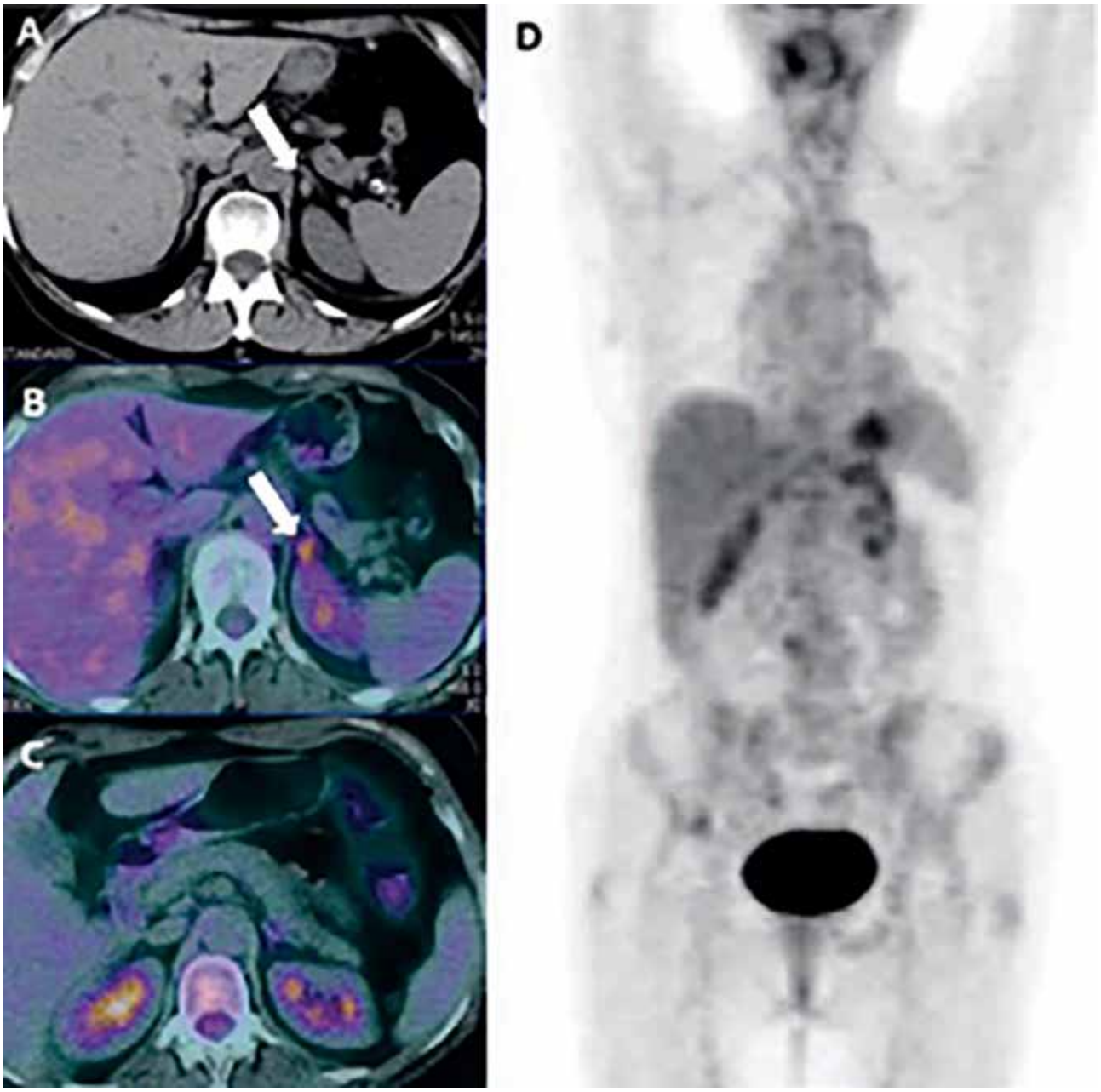

Figure 11. Increased 18F-FDG metabolic activity shows lymphoma of the left adrenal gland (arrow) on axial unenhanced CT (A) and 18F-FDG PET/CT (B). Resolution of the disease after chemotherapy is determined on axial PET/CT (C) and coronal PET (D) images. (Cistaro A, Asabella AN, Coppolino P, Quartuccio N, Altini C, Cucinotta M, Alongi P, Balma M, Sanfilippo S, Buschiazzo A et al. Diagnostic and prognostic value of 18F-FDG PET/CT in comparison with morphological imaging in primary adrenal gland malignancies – a multicenter experience. Hell J Nucl Med 2015; 18(2): 97-102)

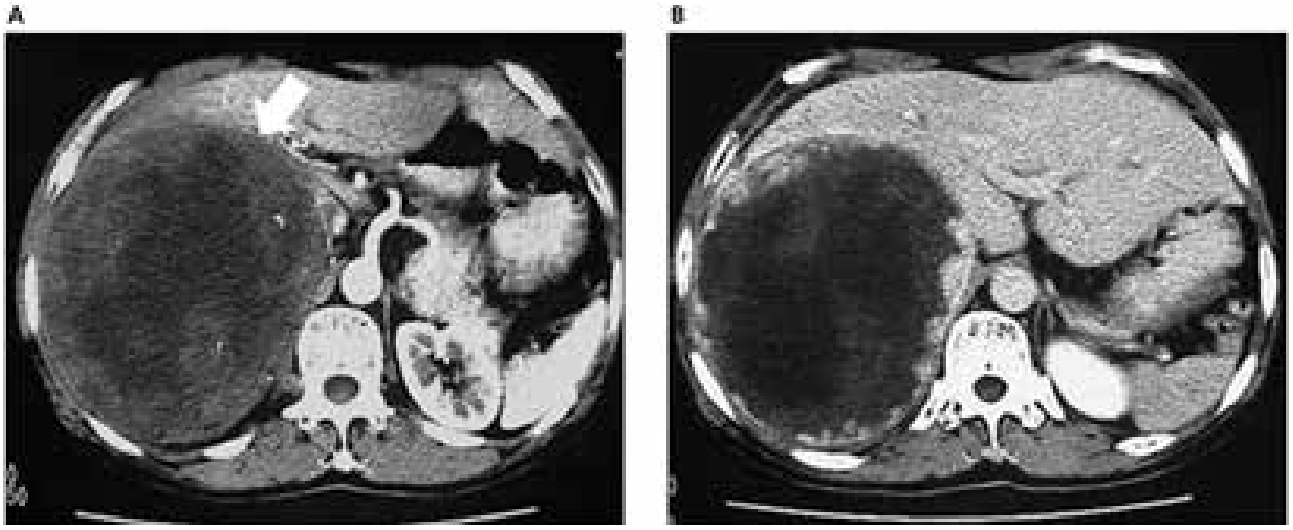

Figure 12. On axial DCE-CT, slight irregular peripheral enhancement and small calcifications during the arterial phase and more intense peripheral enhancement during the delayed phase within a mass (arrow) suggests a cavernous hemangioma of the right adrenal gland. (Xu HX, Liu GJ. Huge cavernous hemangioma of the adrenal gland. J Ultrasound Med 2003; 22: 523-526)

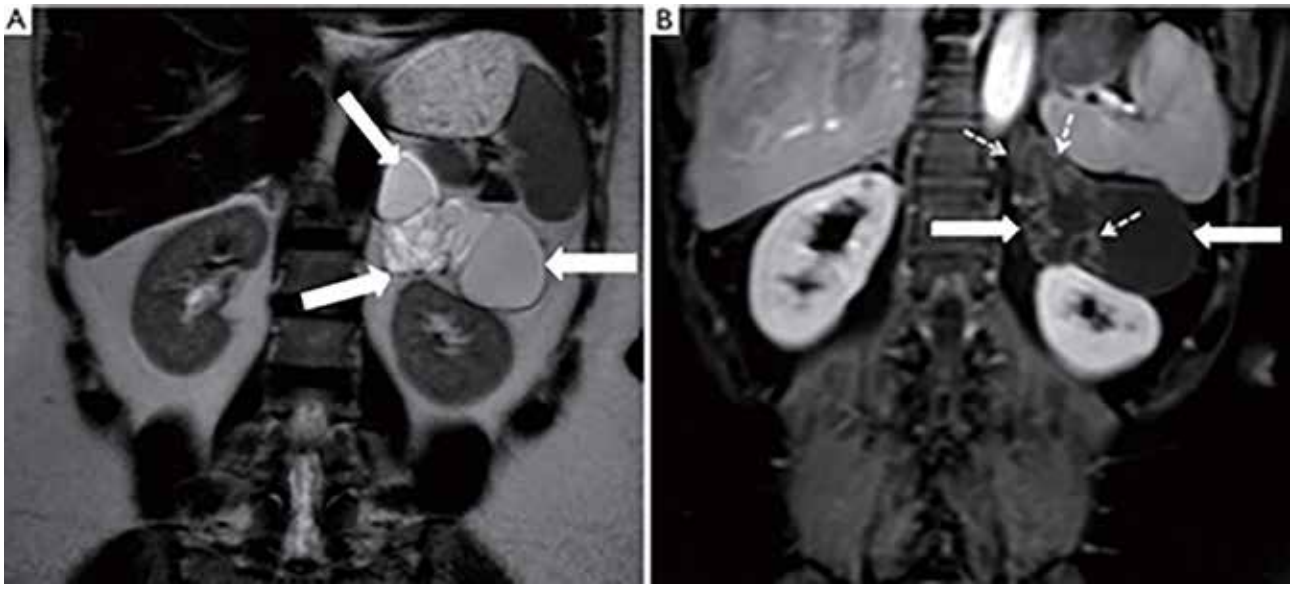

Figure 13. Coronal T2W MRI shows a multiloculated cyctic mass (arrows) in the left adrenal gland (A). On contrast-enhanced fat-saturated T1W MRI, only enhancement of intratumoral septations (dashed arrows) is seen (B). Findings are characteristic of adrenal lymphangioma. (Secil M, Demir O, Yorukoglu K. MRI of adrenal lymphangioma: a case report. Quant Imaging Med Surg 2013; 3(6): 347-348)

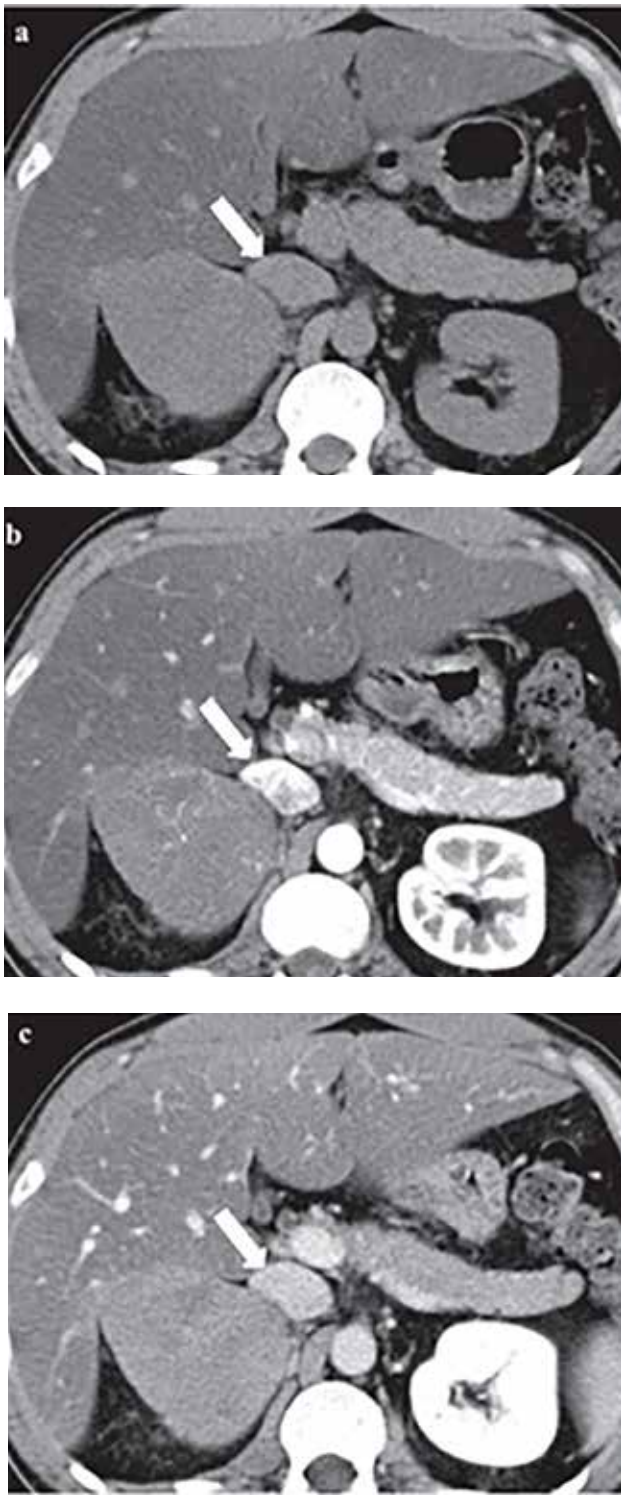

Figure 14. A well-defined homogeneous lesion (arrow) is displayed on axial native CT (A). After injection of the contrast material, slight enhancement of the tumor is observed during arterial phase (B) and delayed phase (C). These features are indicative of Schwannoma. (Suzuki K, Nakanishi A, Kurosaki Y, Nogaki J, Takaba E. Adrenal schwannoma: CT and MRI findings. Radiat Med 2007; 25: 299-302)

DISCUSSION

Adrenocortical adenomas are the most common adrenal neoplasms [3, 24]. These tumors are smaller than others [17, 25, 26] and they usually do not expand. In the case of adrenal adenoma, the mass is observed with cross-sectional imaging over time to detect possible changes in size. An increase of 1 cm is associated with a three times higher risk of a tumor being non-adenomatous [17].

On US, the findings are not specific. Adrenal adenoma is depicted as a small, well-defined solid lesion in the suprarenal region [27].

Histologically, adenoma contains a relatively high amount of intracytoplasmic lipid. This structural particularity is associated with lower attenuation value on native CT. A threshold of 10 HU is used to distinguish adenomas from non-adenomas. However, the quantity of intracellular fat may vary. As a result, imaging findings also differ. The majority of lipid-rich adenomas present as round hypoattenuating (< 10 HU) masses with regular margins on unenhanced CT [28, 29], contrary to lipid-poor adenomas and non-adenomatous tumors (> 10 HU) [25]. It is difficult, yet essential to separate lipid-poor adenomas from malignant lesions due to further diagnostic and treatment strategy. The presence of hyperdense foci (> 10 HU) within a mass requires more detailed assessment.

It should be noted that the 10 HU threshold has high sensitivity, although it lacks specificity. As stated by Iniguez-Ariza et al., a limit of 20 HU would decrease the number of false positive scans [7].

Moreover, the analysis of an unenhanced CT histogram is superior to the assessment of unenhanced mean attenuation. The former has higher sensitivity; a threshold of > 10% negative pixels is used for identifying adenoma [30, 31].

While hyperattenuating lipid-poor adenomas are difficult to differentiate from non-adenomatous lesions on native CT, they respond to contrast enhancement similarly to hypodense lipid-rich adenomas [25]. Higher enhancement, earlier and more rapid enhancement washout suggests adenomatous, either lipid-rich or lipid-poor, a tumor on DCE-CT (Figure 1) [12, 13, 25]. Still,

comparing lipid-rich adenomas to those containing a small amount of lipid, the former has slightly lower enhanced attenuation values, as well as delayed contrast-enhanced attenuation values [12, 25, 32].

There is minor overlap between washout patterns of adenomas and non-adenomas [12]. Hence, they are not pathognomonic.

For 10-min delayed CT, the thresholds of APW and RPW are 50% and 40%, respectively, indicating adrenocortical adenoma [33]. For 15-min delayed CT, the thresholds are 60% and 40%, accordingly [13, 25, 34, 35]. However, RPW and 15-min delayed CT is shown to be more precise [12, 17, 33]. RPW is usually lower in lipid-poor adenomas [32].

Perfusion CT is beneficial in the separation of adenomatous and non-adenomatous lesions as well; the adenomas demonstrate larger blood volume values [36, 37]. Nonetheless, perfusion CT is inferior to washout CT.

Considering that adrenal adenomas contain a relatively large amount of lipid, CS-MRI has become a valuable tool for discriminating them from the other tumors [38, 39]. Adenoma can be determined by decreased SI on T1-weighted (T1W) opposed-phase images compared to T1W in-phase images [40–44]. Indeed, this technique is less appropriate for lipid-poor adenomas.

Quantitative parameters can also be calculated using intratumoral SI on the in-phase and opposed-phase images. Adrenal-to-spleen ratio (ASR) and SI index (SII) are shown to be the most reliable parameters for the separation of adenomas and non-adenomas on CS-MRI [45]. ASR < 0.71 or SII > 16.5% is suggestive of lipid-rich adenoma [46, 47]. However, SII is more precise than ASR [47]. Considering the diagnostic possibilities of CS-MRI, it is far more superior to unenhanced CT [46], yet inferior to DCE-CT [48], especially for the characterization of lipid-poor adenomas. CS-MRI has a remarkable sensitivity if the attenuation value of the lesion is < 20 HU on native CT. In other cases, the sensitivity decreases [49].

A substantial overlap of apparent diffusion coefficient (ADC) values in adenomatous and non-adenomatous tumors are observed on DW-MRI [42, 50].

On dynamic contrast-enhanced MRI (DCE-MRI), the adrenocortical adenoma can be depicted by homogeneous enhancement on the arterial phase or capillary blush (increased SI higher than liver) with rapid washout on the venous phase [41, 43, 51]. In the case of lipid-poor adenoma, DCE-MRI is more valuable than CS-MRI due to inadequate SI loss on the opposed-phase. On the other hand, it should be used carefully in patients with decreased renal function owing to possible gadolinium-induced nephrogenic systemic fibrosis [52].

Lower 18F-FDG uptake of the lesion compared to uptake of the liver parenchyma indicates an adenoma on PET/CT [23, 53]. Still, there is a moderate overlap of 18F-FDG metabolic activity between adenomas and non-adenomas, e.g., hormone-secreting adenomas or those with large amounts of intracytoplasmic lipofuscin can mimic malignant adrenal neoplasms due to increased 18F-FDG uptake [54, 55].

Myelolipoma is the second most frequent adrenal incidentaloma [3]. It is always benign and mostly consists of adipocytes with some hematopoietic elements. However, fat is not an imperative element of the lesion. Although the majority of tumors are found in the adrenal gland, extra-adrenal myelolipomas are also identified [56–59].

Myelolipomas are encapsulated or have definite margins [60]. Atypical findings are hemorrhage or calcification within the mass [61–63]. They grow relatively slowly [64]. Nonetheless, the tumors tend to become larger; those who exceed 10 cm in diameter are known as giant myelolipomas. Bigger masses are likely to rupture and produce hematomas [65].

On US, myelolipoma is depicted as a heterogeneous hyperechoic or isoechogenic mass in the suprarenal region [62, 66–68]. Heterogenicity is a result of the variable architecture of the lesion. Low attenuation is characteristic of myeloid components. Therefore, hemopoietic cells determine the presence of hypoechogenic foci within the lipomatous tumor [68, 69].

Supersonic shear wave elastography may help distinguish myelolipomas from other benign adrenal masses; myelolipomas are harder than nodular hyperplasia or adenomas [70]. However, the US is insufficient in the diagnosis of myelolipoma.

A round or oval well-circumscribed heterogeneous hypodense lesion is observed in a case of myelolipoma on unenhanced CT [71, 72]. Negative attenuation values imply the presence of fat [68]. Hence, the attenuation of the tumor depends on the amount of the adipose tissue (Figure 2).

Mild enhancement is detected in the hematopoietic regions after the injection of the contrast material [72, 73].

On MRI, features typical of myelolipoma might vary. On T1W images, it can present as a homogeneous hyperintense or hypointense (if myeloid components predominate) mass with regular margins [71, 74]. On T2W images, high or intermediate SI is observed [22, 71].

Using fat-saturated T2W images, loss of SI within the fat allows identifying myelolipoma (Figure 3) [72].

A signal drop, which indicates the presence of adipose tissue, is also seen on opposed-phase CS-MRI [74].

Gadolinium-enhanced MRI displays mild enhancement of the tumor [72].

Metabolic activity of 18F-FDG is lower in fat compared to myeloid tissue [75]. Consequently, the uptake of 18F-FDG is usually not increased on PET/CT [76].

Pheochromocytoma is a rare adrenomedullary tumor derived from chromaffin cells. Extra-adrenal pheochromocytomas, termed as paragangliomas, arise from paraganglionic chromaffin cells in the sympathetic nervous system. Most patients with chromaffin-derived neoplasms have hereditary or de novo germline mutations in one of the susceptibility genes [77].

A portion of these masses secrete catecholamines. Thus, they can precipitate headache, cardiac arrhythmias or life-threatening hypertension since adrenergic crisis may occur during percutaneous biopsy [78, 79]. Laboratory tests along with radiological imaging play an essential role in the determination of pheochromocytoma and its function.

On native CT, around homogeneous or, mostly, heterogeneous lesion with possible calcification, cystic or hemorrhagic changes is observed in a case of pheochromocytoma [80–83]. Cystic degeneration and necrosis are more common in larger masses [84]. The attenuation of pheochromocytoma is usually > 10 HU, and it does not significantly differ from the attenuation of lipid-poor adenoma [81, 85, 86]. However, compared to lipid-poor adenomas, pheochromocytomas are more extensive [85, 86]. If a malignant transformation has occurred, metastases in the regional lymph nodes or liver parenchyma can be detected [87].

DCE-CT is recommended as the first-line imaging tool in patients with suspected adrenomedullary neoplasm [88]. On DCE-CT, pheochromocytoma presents as a heterogeneous hyperdense lesion; its attenuation is higher than of adenoma [34, 86, 89]. Regions with no enhancement can be noticed if cystic or necrotic changes are present (Figure 4) [81]. The contrast agent washout of this tumor is variable. Lower APW and RPW are representative of pheochromocytoma rather than of adrenal adenoma [86]. Nonetheless, it can frequently imitate adenoma due to a similar washout pattern [81, 82, 84]. As stated by Woo et al., 35% of pheochromocytomas display early contrast enhancement and washout with coinciding APW and RPW [90]. Thus, the exclusion of this tumor should not be based only on the findings of the DCE-CT.

On T1W images, pheochromocytoma is hypointense. On T2W images, it is depicted as a solid, hypervascular, hyperintense mass [80]. However, it can mimic other benign or malignant tumors due to atypical features, such as fat, hemorrhage, cysts or calcification.

CS-MRI is also beneficial; SII < 16.5% and ASR SI ratio > 0.71 imply pheochromocytoma [86]. Nonetheless, if a tumor is larger, an SI drop correlating to a higher amount of intracytoplasmic lipid can be observed on opposed-phase images.

DW-MRI may help differentiate pheochromocytomas from adenomas. The use of ADC in separating adrenal neoplasms has been debatable [91–93]. However, a new study shows that evaluating the heterogenicity of diffusion is more accurate. According to Umanodan et al., increased entropy of ADC values is characteristic to pheochromocytomas rather than adenomas [94]. Hemorrhage, necrosis or cystic changes are more frequent in pheochromocytomas, and these features determine the heterogenicity of the tumor. Therefore, a wider range of ADC values is seen in

the ADC histogram.

Avid heterogeneous enhancement is characteristic to pheochromocytoma on T1W gadolinium-enhanced images.

On PET/CT, pheochromocytoma is recognized by high uptake intensity compared to the liver parenchyma, regardless of the radioactive tracer (Figure 5) [95]. Still, 18F-FDG is the tracer of choice in diagnosing this adrenomedullary tumor [96]. Metabolic activity of the lesion helps to make a distinction between a benign and malignant pheochromocytoma. The latter is larger and has a higher 18F-FDG maximum standardized uptake value (SUVmax) [97].

Iodine-131-metaiodobenzylguanidine (131I-MIBG), another tracer, is taken up by catecholamine-secreting tumors. Thus, it is useful in the diagnosis of pheochromocytoma. 131I-MIBG, being a pharmacologic analog of guanethidine and norepinephrine, competes with endogenic amines in adrenergic tissues.

18F-FDG and 131I-MIBG scans complement one another in the identification of pheochromocytomas [97]. However, 18F-FDG PET/CT has higher sensitivity in detecting the dissemination of the disease [77]. Therefore, it should be used if the metastatic spread is suspected [88]. 18F-FDG PET/CT is useful in the diagnosis of pheochromocytoma, yet this imaging technique is inferior to CT or MRI [98].

Radioisotope gallium-68-DOTA-tyr3-octreotate (68Ga-DOTATATE) is presumably superior to 18F-FDG and 131I-MIBG. The use of 68Ga-DOTATATE PET/CT in conjunction with 18F-FDG PET/CT is beneficial in patients with the aggressive phenotype of the disease. In such a case, low 68Ga-DOTATATE and high 18F-FDG uptake are observed [95].

PET/CT with fluorine-18-dihydroxyphenylananine (18F-DOPA) is valuable as well. As stated by Fiebrich et al., it is more sensitive than other imaging techniques in distinguishing catecholamine-secreting masses. Moreover, the metabolic activity of 18F-DOPA correlates with plasma and urine normetanephrine [99].

In spite of that, the uptake of radioactive tracers is predisposed not only by the location, malignancy or secretory function of pheochromocytoma but also by the underlying genetic status [97, 100–102]. Consequently, the results of genetic testing should be taken into consideration while evaluating PET/CT images.

Primary carcinoma of the adrenal gland is a rare tumor, often found incidentally. Nevertheless, abdominal pain or a palpable mass can be present. Moreover, endocrine dysfunction, such as virilization, feminization or Cushing's syndrome, is frequently observed in patients with adrenocortical carcinoma [103, 104].

The prognosis of adrenal carcinoma is poor; the 5-year survival rate is approximately 50% [104, 105]. Older age, more significant lesion and metastatic spread is associated with malignancy and lower survival rate [7, 105].

Radiologic imaging enables to diagnose this aggressive neoplasm. On the US, a heteroechoic mass is detected in the adrenal gland [106].

On unenhanced CT, carcinoma presents as a round, oval or lobulated heterogeneous mass [107, 108]. The attenuation values of carcinoma are higher than of adenoma, although there is an overlap [28, 109]. Adrenocortical carcinoma may have a central hypodense region due to hemorrhage or necrosis (Figure 6). Additionally, hyperdense areas owing to calcification can be seen [110]. Infiltration to the adjacent tissue, including inferior vena cava liver or kidney, adenopathy, and metastasis helps to differentiate carcinoma from a benign tumor [110, 111].

After the injection of the contrast agent, inhomogeneous peripheral enhancement of the lesion is indicative of carcinoma [110]. RPW < 40% is consistent with malignancy [111, 112].

CT 3D reconstruction of the malignant lesion is valuable for evaluating its invasion and choosing the most suitable surgery plan [113, 114].

MRI is another useful imaging tool. A heterogeneous hyperintense mass is observed in a case of carcinoma on T1W and T2W images [22, 115, 116].

Intracytoplasmic lipid is not typical. Nonetheless, fatty regions within the tumor may be present in some cases. Thus, foci of decreased SI are seen on opposed-phase images.

18F-FDG PET/CT offers high diagnostic performance in separating malignant adrenal masses [26, 117]. Intense heterogeneous metabolic activity of 18F-FDG suggests carcinoma [115].

Using carbon-11-metomidate (11C-MTO) as a tracer, carcinoma can be differentiated from other adrenal lesions on PET. Extremely increased uptake of this radioactive isotope is characteristic of carcinoma, whereas pheochromocytoma and metastasis are 11C-MTO negative [118, 119]. Regions lacking the 11C-MTO uptake correlate to necrosis within the tumor (Figure 7). Nuclear medicine also contributes to the staging of the disease and follow-up after the treatment [120–122].

Primary tumors that disseminate to the adrenal glands are usually found in the lungs and esophagus [123–126]. Adrenal metastases are significantly larger than benign adrenal masses [127]. Nonetheless, other radiologic findings associated with malignancy are more valuable for diagnosis [124].

The US has low sensitivity in differentiating adrenal lesions. Still, it can be used, if other radiologic techniques are contraindicated. The metastatic tumor is recognized by its hypoechogenicity. On contrast-enhanced endoscopic US (CE-EUS), it appears as a hypervascular mass during the early vascular phase with delayed enhancement [128].

Adrenal metastasis presents as a solid hyperdense mass with smooth or irregular margins on native CT [123, 127, 129]. The majority of metastases are heterogeneous. However, this feature is not pathognomic [129, 130]. Regional lymphadenopathy, thrombosis of the renal vein or inferior vena cava and invasion of the adjacent tissues also allows differentiating malignant lesions from the benign ones. Furthermore, they show a higher and more rapid increase in size than benign lesions on follow-up images [129].

On DCE-CT, heterogeneous peripheral enhancement is observed [130].

Heterogeneous mass that is isointense on T1W images and hyperintense on T2W images implies the presence of metastasis.

CS-MRI demonstrates an insignificant signal drop on the opposed-phase images [43].

Gadolinium-enhanced MRI shows moderate and persistent peripheral enhancement without washout suggestive of metastasis [41, 43].

PET/CT is a precise, non-invasive imaging technique, although it has a lower accuracy than DCE-CT [23]. A combination of washout CT and PET/CT is more accurate for the identification of metastasis than these imaging tools separately [123]. 18F-FDG uptake is higher or equal that of the liver in patients with metastatic foci (Figure 8) [21, 131–133]. These masses have higher 18F-FDG metabolic activity than benign lesions [21, 23]; SUVmax > 2.5 is characteristic of metastasis [125, 126, 134]. In some cases, the low metabolic activity of the radioisotope may be observed. This finding is associated with necrotic, hemorrhagic or especially small metastases [135].

A broad spectrum of masses, other than pheochromocytoma, arises from adrenomedullary ganglion cells. One of them, ganglioneuroma is a benign tumor. It originates from neural crest cells and consists of Schwann cells, ganglion cells, and nerve fibers. The majority of these masses are asymptomatic, therefore, they are found incidentally [136–138]. In other cases, patients experience abdominal discomfort or hypertension [137].

The radiologic features of ganglioneuroma are non-specific. On the US, it is depicted as a well-defined hypoechoic lesion, usually > 3 cm in size [136].

The blood flow signal is not established on Color Doppler US [136].

Unenhanced CT provides more information about the adrenal pathology. An oval or lobulated encapsulated lesion of low-attenuation, yet > 10 HU, is observed in patients with ganglioneuroma [136, 138–140]. Its homogeneity depends on the different proportions of Schwann cells and ganglions. CT may also display either central or peripheral speckled calcifications [136, 137, 140–142].

After the injection of the iodine-based contrast, low to intermediate delayed heterogeneous enhancement suggests a ganglioneuroma [136, 137, 142, 143].

Low SI on T1W images and high SI on T2W images are typical of ganglioneuroma (Figure 9) [136, 138, 139, 141, 144]. Nonetheless, it does not allow to differentiate ganglioneuroma from other neurogenic tumors.

DCE-MRI demonstrates weak delayed enhancement, as seen on DCE-CT [145, 146]. Still, MRI is inferior to CT owing to the ability of the latter

to showcase intratumoral calcifications [147].
Nuclear medicine can help identify the lesion, although the findings are not pathognomic. Metabolic activity of 18F-FDG is frequently mildly increased [136, 142, 146], yet ganglioneuroma sometimes does not take up the radioisotope at all [138].
If 131I-MIBG is used as a tracer, increased uptake can be observed.
Another tumor that originates from neural crest cells is neuroblastoma. It is a malignant mass common in the pediatric population [1]. Clinical symptoms characteristic of the tumor are irregular fever, abdominal pain or a palpable mass [148–150]. Neuroblastomas are extremely aggressive; the five-year overall survival rate is 50.8% [150]. However, in rare cases, neuroblastoma may undergo histological maturation into a benign ganglioneuroma [151].
A solid heterogeneously echoic lesion or an anechoic cystic mass is displayed on the US [152–156]. Bright echoes with acoustic shadowing, indicative of calcifications, may also be detected [156].
Native CT allows assessing the mass more scrupulously. Heterogeneous hypodense irregularly-shaped mass with granular calcifications is suggestive of neuroblastoma. Additionally, necrosis or cystic changes are frequent findings. Features, associated with malignancy, such as infiltration of the adjacent organs and lymphatic metastases, are also typical (Figure 10) [148].
Moderate inhomogeneous enhancement, except for the regions of necrosis and cystic changes, is seen on contrast-enhanced CT [148, 157].
On MRI, neuroblastoma presents as hypointense on T1W images and hyperintense on T2W images, identical to ganglioneuroma [149, 158, 159].
On gadolinium-enhanced MRI, heterogeneous enhancement of the mass is recognized [158].
Scintigraphy with 123MIBG or 131MIBG has become a valuable tool for the identification and staging of malignant neural crest tumors [160]. Increased MIBG uptake is determined in patients with neuroblastoma [161, 162]. Although, a false-negative scan may be occasionally observed [162]. Thus, 18F-FDG PET is recommended owing to its higher sensitivity [163]. According to Kroiss et al., gallium-68-DOTA-tyr3-octreotide (68Ga-DOTATOC) PET could also be helpful [164]. However, integrated imaging of MRI and PET further increases the accuracy in diagnosing neuroblastomas [165].
Ganglioneuroblastoma is a transitional mass which contains cells of both benign ganglioneuroma and malignant neuroblastoma. It is less differentiated than ganglioneuroma and is more related to neuroblastoma by its aggressive behavior. The main distinction between these two tumors is the regular margins of ganglioneuroblastoma and lower CT attenuation value due to its hypocellularity compared to neuroblastoma. Moreover, metastases are also more frequently observed in patients with neuroblastomas [166].
Imaging features of ganglioneuromas, ganglioneuroblastomas, and neuroblastomas do not significantly differ. Consequently, distinguishing neural crest tumors is possible only by a histological examination. However, a study shows that DW-MRI can be useful to separate these lesions. They are all hyperintense on DW-MRI. Nonetheless, ADC of malignant lesions is higher than of the benign ones [167].
Adrenal lymphoma, a rare tumor, can be primary or secondary. The most common histological type is non-Hodgkin lymphoma. Adrenal lymphoma occurs in 4% of the patients with non-Hodgkin lymphoma [168]. The mass usually presents with atypical symptoms, such as abdominal pain, fever or weight loss [169–171].
Radiologic imaging plays a notable role in the identification of the lesion. A heterogeneous hypoechoic mass with feasible hepatosplenomegaly can be determined on the US [172, 173]. However, the US lacks sensitivity in differentiating lymphoma from other adrenal malignant tumors.
On native CT, lymphoma is recognized as a round, oval or lobulated mass which is hypodense compared to the liver parenchyma, yet its attenuation value is > 10 HU [169, 174–176]. Rarely, calcifications within the mass can be seen [177]. Lymphoma is usually a well-defined lesion without invasion of the adjacent organs [178].
DCE-CT shows a slight gradual, heterogeneous enhancement [174, 175, 179].
Low to intermediate SI on MRI T1W images and high SI on T2W images is characteristic of adrenal lymphoma [178].

Using CS-MRI, a loss of SI is not visualized on opposed-phase images [174].
DW-MRI displays restricted diffusion within the lesion [179, 180].
On gadolinium-enhanced MRI, solid mass with homogeneous or heterogeneous contrast enhancement implies lymphoma [178–180]. In some cases, enlargement of the regional lymph nodes is established [181, 182].
PET/CT has higher accuracy in the differentiation of adrenal lymphoma than DCE-CT [117]. PET/CT images show avid 18F-FDG uptake in patients with lymphoma (Figure 11) [174, 183–185].
Cavernous hemangioma is an uncommon pathology of the adrenal gland; it usually affects skin and liver. Hemangioma is a benign vascular mass that consists of angioblastic cells. Due to their absent clinical manifestation, only enlarged (> 10 cm) hemangiomas are diagnosed clinically. Unfortunately, large hemangiomas may rupture and cause retroperitoneal hemorrhage, leading to hypotension [186].
Radiologic imaging determines the lesion accidentally in most cases. On the US, hemangioma appears as a well-defined hyperechoic inhomogeneous solid lesion in the suprarenal area [187, 188]. However, some patients present with a lesion that consists of diffuse anechoic regions with hyperechoic septa [189]. Intratumoral calcified foci may also be observed [188].
On unenhanced CT, a heterogeneous hypoattenuated lesion with regular margins and peripheral calcifications is characteristic of hemangioma [190–196].
The mass with the hypodense center is displayed on DCE-CT [192, 197]. Early irregular peripheral enhancement with enhancement extending to the center of the lesion during the delayed phase suggests an adrenal hemangioma (Figure 12) [189].
MRI does not show high sensitivity in the diagnosis of the tumor. The findings are non-specific, i.e., hemangioma is hypointense on T1W images and hyperintense on T2W images [187, 188, 198]. Regions of high SI within the mass are indicative of hemorrhage or calcification [190].
On opposed-phase CS-MRI, SI does not change significantly [190].
The enhancement pattern on DCE-MRI is similar to that on DCE-CT; early peripheral rim-like enhancement with slow patchy centripetal enhancement is determined [189, 190].
Lymphangioma is another benign tumor. Histologically, it is composed of multicystic owing to irregular dilated lymphatic vessels [199]. Lymphangiomas are frequently found in the neck, axilla, and mediastinum; adrenal lymphangioma is an extremely rare pathology. Adrenal masses are usually asymptomatic. However, abdominal or back pain can be present [199].
The US, as a primary imaging method, depicts the tumor as a well-defined multilocular anechoic cystic lesion [200–202].
Adrenal lymphangioma should be included in the differential diagnosis if a well-circumscribed hypodense mass with subtle septal structures is observed on native CT scans [203, 204]. Attenuation values are similar to those of lipid-rich adenomas. Nonetheless, only septal enhancement is seen after the administration of the contrast material in patients with lymphangioma [201, 204, 205]. Moreover, peripheral curvilinear or punctate calcifications may be recognized within lymphangiomas, contrary to adenomas [200, 204].
Lymphangioma appears hypointense on MRI TW1 images and hyperintense on T2W images [206–208].
On gadolinium-enhanced MRI, isolated septal enhancement is typical of the tumor, correspondingly to DCE-CT images (Figure 13) [202].
Although radiologic imaging has become highly informative in distinguishing the adrenal tumors, malignant lesions remain in the differential diagnosis, if lymphangioma is present.
Adrenal schwannoma is a slowly growing benign mass. It arises from Schwann cells of myelinated sympathetic nerve fibers that innervate the adrenal medulla. Histologically, these tumors have two principal microscopic patterns of growth. The Antoni A pattern is highly cellular, the Antoni B pattern is composed of myxoid and hyaline degeneration. The tumor is usually asymptomatic [209–211]. When large, schwannomas develop degenerative (hemorrhagic or cystic) changes. These degenerative lesions are known as ancient schwannomas.
Schwannoma is frequently found incidental-

ly during the US examination. It is displayed as a hypoechoic mass with definite margins [212, 213].

On native CT, non-specific findings are observed in patients with adrenal schwannoma. The lesion is well-circumscribed heterogeneous and low-attenuated [214, 215]. Septa, cystic changes and calcification related to the tumor wall may be identified [214, 216, 217]. In such cases, schwannoma mimics a malignant tumor.

On DCE-CT, mild heterogeneous contrast enhancement during the hepatic arterial phase with progressive enhancement during the portal vein phase implies the presence of schwannoma (Figure 14) [212, 214, 215, 218].

Schwannoma is hypointense to isointense on MRI T1W images. On T2W images, it is inhomogeneous and hyperintense [211, 215, 218, 219]. T2W images are more informative; higher SI is characteristic of predominant Antoni B tissue rather than of Antoni A tissue [220].

The chemical shift sequence does not show a signal drop on opposed-phase images [215].

On DCE-MRI, schwannoma is identified by early enhancement without significant washout [221].

PET/CT demonstrates increased homogeneous or heterogeneous 18F-FDG uptake [222].

In conclusion, non-invasive radiologic imaging allows identifying typically asymptomatic tumors of the adrenal gland. Adrenal CT protocol is the most reliable technique in the differentiation of these diverse neoplasms. On the other hand, CS-MRI is indispensable for verifying intratumoral lipomatous components and, consequently, selecting the most appropriate approach to manage the mass. Furthermore, PET/CT permits characterizing indeterminate tumors and their potential metastatic spread. Nonetheless, some neoplasms do not display specific features and cannot be distinguished only based on radiologic imaging. Hence, clinical symptoms, laboratory test, and biopsy are essential for making a correct diagnosis.

REFERENCES

1. Lin X, Wu D, Chen C, Zheng N. Clinical characteristics of adrenal tumors in children: a retrospective review of a 15-year single-center experience. Int Urol Nephrol 2017; 49: 381–385.

2. Ahn SH, Kim JH, Baek SH, Kim H, Cho YY, Suh S, Kim BJ, H S, Koh JMK, Lee SH et al. Characteristics of adrenal incidentalomas in a large, prospective computed tomography-based multicenter study: the COAR study in Korea. Yonsei Med J 2018; 59(4): 501–510.

3. Bovio S, Cataldi A, Reimondo G, Sperone P, Novello S, Berruti A, Borasio P, Fava C, Dogliotti L, Scagliotti GV et al. Prevalence of adrenal incidentaloma in a contemporary computerized tomography series. J Endocrinol Invest 2006; 29: 298-302.

4. Paulsen SD, Nghiem HV, Korobkin M, Caoili EM, Higgins EJ. Changing role of imaging-guided percutaneous biopsy of adrenal masses: evaluation of 50 adrenal biopsies. AJR 2004; 182: 1033–1037.

5. Azoury SC, Nagarajan N, Young A, Mathur A, Prescott JD, FIshman EK, Zeiger MA. Computed tomography in the management of adrenal tumors: does size still matter? J Comput Assist Tomogr 2017; 41: 628–632.

6. Foo E, Turner R, Wang KC, Aniss A, Gill AJ, Sidhu S, Clifton-Bright R, Sywak M. Predicting malignancy in adrenal incidentaloma and evaluation of a novel risk stratification algorithm. ANZ J Surg 2018; 88: E173–177.

7. Iniguez-Ariza NM, Kohlenberg JD, Delivanis DA, Hartman RP, Dean DS, Thomas MA, Shah MZ, Herndon J, McKenzie TJ, Arlt W et al. Clinical, biochemical, and radiological characteristics of a single-center retrospective cohort of 705 large adrenal tumors. Mayo Clin Proc Inn Qual Out 2018; 2(1): 30–39.

8. Delivanis DA, Bancos I, Atwell TD, Schmit GD, Eiken PW, Natt N, Erickson D, Maraka S, Young Jr WF, Nathan MA. Diagnostic performance of unenhanced computed tomography and 18F-fluorodeoxyglucose positron emission tomography in indeterminate adrenal tumours. Clin Endocrinol (Oxf) 2018; 88: 30–36.

9. Mohamed RE, Sherif MF, Amin A. Differentiation of adrenal incidentalomas by qualitative and quantitative analytical data obtained by 18F-FDG positron emission tomography/ computed tomography in cancer patients. Egypt J Radiol Nucl Med 2018; 49: 764–775.

10. Dinnes J, Bancos I, Di Ruffano LF, Chortis V, Davenport C, Bayliss S, Sahdev A, Guest P, Fassnacht M, Deeks JJ et al. Imaging for the diagnosis of malignancy in incidentally discovered adrenal masses: a systematic review and meta-analysis. Eur J Endocrinol 2016; 175: R51-R64.

11. Mayo-Smith WW, Song JH, Boland GL, Francis IR, Israel GM, Mazzaglia PJ, Berland LL, Pandharipande PV. Management of incidental adrenal masses: a white paper of the ACR incidental findings committee. J Am Coll Radiol 2017; 14: 1038–1044.

12. Wang X, Li K, Sun H, Zhao J, Zheng L, Zhang Z, Bai R, Zhang G. Differentiation between adrenal adenomas and nonadenomas using dynamic contrast-enhanced computed tomography. Onco Targets Ther 2016; 9: 6809–6817.

13. Korobkin M, Brodeur FJ, Francis IR, Quint LE, Dunnick NR, Londy F. CT time-attenuation washout curves of adrenal adenomas and nonadenomas. AJR 1998; 170: 747–752.

14. Song J, Zhang C, Liu Q, Yu T, Jiang X, Xia Q, Zhang Y, Sequeiros RB. Utility of chemical shift and diffusion-weighted imaging in characterization of hyperattenuating adrenal lesions at 3.0T. Eur J Radiol 2012; 81: 2137–2143.

15. Leroy-Willig A, Bittoun A, Luton JP, Louvel A, Lefevre JE,

Bonnin A, Roucayrol JC. In vivo MR spectroscopic imaging of the adrenal glands: distinction between adenomas and carcinomas larger than 15 mm based on lipid content. AJR 1989; 153: 771–773.

16. Wu YW, Tan CH. Determination of a cutoff attenuation value on single-phase contrast-enhanced CT for characterizing adrenal nodules via chemical shift MRI. Abdom Radiol 2016; 41: 1170–1177.

17. Koo HJ, Choi HJ, Kim HJ, Kim SO, Cho KS. The value of 15-minute delayed contrast-enhanced CT to differentiate hyperattenuating adrenal masses compared with chemical shift MR imaging. Eur Radiol 2014; 24: 1410–1420.

18. El-Kalioubie M, Emad-Eldin S, Abdelaziz O. Diffusion-weighted MRI in adrenal lesions: a warranted adjunct? Egypt J Radiol Nucl Med 2016; 47: 599–606.

19. Guerin C, Pattou F, Brunaud, Lifante JC, Mirallie E, Haissaguerre M, Huglo D, Olivier P, Houzard C, Ansquer C et al. Performance of 18F-FDG PET/CT in the characterization of adrenal masses in noncancer patients: a prospective study. J Clin Endocrinol Metab 2017; 102(7): 2465–2472.

20. Han SJ, Kim TS, Jeon SW, Jeong SJ, Yun M, Rhee Y, Kang ES, Cha BS, Lee EJ, Lee HC et al. Analysis of adrenal masses by 18F-F-FDG positron emission tomography scanning. Int J Clin Pract 2007; 61(5): 802–809.

21. Erasmus JJ, Patz Jr EF, McAdams HP, Murray JG, Herndon J, Coleman RE, Goodman PC. Evaluation of adrenal masses in patients with bronchogenic carcinoma using 18F-fluorodeoxyglucose positron emission tomography. AJR 1997; 168: 1357–1360.

22. Maurea S, Mainolfi C, Bazzicalupo L, Panico MR, Imparato C, Alfano B, Ziviello M, Salvatore M. Imaging of adrenal tumors using FDG PET: comparison of benign and malignant lesions. AJR 1999; 173: 25–29.

23. Park BK, Kim CK, Kim B, Choi JY. Comparison of delayed enhanced CT and 18F-FDG PET/CT in the evaluation of adrenal masses in oncology patients. J Comput Assist Tomogr 2007; 31(4): 550–556.

24. Song JH, Chaudhry FS, Mayo-Smith WW. The incidental adrenal mass on CT: prevalence of adrenal disease in 1,049 consecutive adrenal masses in patients with no known malignancy. AJR 2008; 190: 1163–1168.

25. Caoili EM, Korobkin M, Francis IR, Cohan RH, Dunnick NR. Delayed enhanced CT of lipid-poor adrenal adenomas. AJR 2000; 175: 1411–1415.

26. Humbert AL, Lecoanet G, Moog S, Bouderraoui F, Bresler L, Vignaud JM, Chevalier E, Brunaud L, Klein M, Cuny T. The computed tomography adrenal wash-out analysis properly classifies cortisol secreting adrenocortical adenomas. Endocrine 2018; 59: 529–537.

27. S. Goyal, Essentials of abdomino-pelvic sonography: a handbook for practitioners. 1st ed. Boca Raton, FL: CRC Press/Taylor & Francis Group, 2018.

28. Thomas AJ, Habra MA, Bhosale PR, Qayyum AA, Ahmed K, Vicens R, Elsayes KM. Interobserver agreement in distinguishing large adrenal adenomas and adrenocortical carcinomas on computed tomography. Abdom Radiol 2018; 43: 3101–3108.

29. Korobkin M, Brodeur FJ, Yutzy GG, Francis IR, Quint LE, Dunnick NR, Kazerooni EA. Differentiation of adrenal adenomas from nonadenomas using CT attenuation values. AJR 1996; 166: 531-536.

30. Ho LM, Paulson EK, Brady MJ, Wong TZ, Schindera ST. Lipid-poor adenomas on unenehanced CT: does histogram analysis increase sensitivity compared with a mean attenuation threshold? AJR 2008; 191: 234–238.

31. Jhaveri KS, Wong F, Ghai S, Haider MA. Comparison of CT histogram analysis and chemical shift MRI in the characterization of indeterminate adrenal nodules. AJR 2006; 187: 1303–1308.

32. Mosconi C, Vicennati V, Papadopoulos D, Di Dalmazi G, Morselli-Labate AM, Golfieri R, Pasquali R. Can imaging predict subclinical cortisol secretion in patients with adrenal adenomas? A CT predictive score. AJR 209; 122–129.

33. Sangwaiya MJ, Boland GWL, Cronin CG, Blake MA, Halpern EF, Hahn PF. Incidental adrenal lesions: accuracy of characterization with contrast-enhanced washout multidetector CT – 10-minute delayed imaging protocol revisited in a large patient cohort. Radiology 2010; 256(2): 504–510.

34. Northcutt BG, Trakhtenbroit MA, Gomez EN, Fishman EK, Johnson PT. Adrenal adenoma and pheochromocytoma: comparison of multidetector CT venous enhancement levels and washout characteristics. J Comput ASsist Tomogr 2016; 40: 194–200.

35. Mohamed RE, Abodewan KA, Amin MA. Diagnostic value of delayed washout rate of contrast-enhanced multi-detector computed tomography in adrenal incidentalomas. Alexandria J Med 2014; 50: 345–358.

36. Qin H, Sun H, Li Y, Shen B. Application of CT perfusion imaging to the histological differentiation of adrenal gland tumors. Eur J Radiol 2012; 81: 502–507.

37. Mohammed AR, Ahmed AT, Khalil TH, Refaie HF. Dynamic perfusion CT parameters and delayed contrast washout CT in characterization of adrenal tumors: a comparative study. Egypt J Radiol Nucl Med 2017; 48: 707–716.

38. Platzek I, Sieron D, Plodeck V, Borkowetz A, Laniado M, Hoffmann RT. Chemical shift imaging for evaluation of adrenal masses: a systematic review and meta-analysis. Eur Radiol 2019; 29(2): 806-817.

39. Hanna S, El-Kalioubie M, Badawy H, Halim M. Optimal diagnosis of adrenal masses. Egypt J Radiol Nucl Med 2015; 46: 511–520.

40. Bilbey JH, McLoughlin RF, Kurkjian PS, Wilkins GEL, Chan NHL, Schmidt N, Singer J. MR imaging of adrenal masses: value of chemical-shift imaging for distinguishing adenomas from other tumors. AJR 1995; 164: 637-642.

41. Chung JJ, Semelka RC, Martin DR. Adrenal adenomas: characteristic postgadolinium capillary blush on dynamic MR imaging. J Magn Reson Imaging 2001; 13: 242–248.

42. Miller FH, Wang Y, McCarthy RJ, Yaghmai V, Merrick L, Larson, Berggruen S, Casalino DD, Nikolaidis P. Utility of diffusion-weighted MRI in characterization of adrenal lesions. AJR 2010; 194: W179–W185.

43. Rodacki K, Ramalho M, Dale BM, Battisti S, de Campos ROP, Giardino A, Semelka RC. Combined chemical shift imaging with early dynamic serial gadolinium-enhanced MRI in the characterization of adrenal lesions. AJR 2014; 203: 99–106.

44. Slapa RZ, Jakubowski W, Januszewicz A, Kasperlik-Zaluska AA, Dabrowska E, Fijuth J, Feltynowski T, Tarnawski R, Krolicki L. Discriminatory power of MRI for differentiation of adrenal non-adenomas vs adenomas evaluated by means of ROC analysis: can biopsy be obviated? Eur Radiol 2000; 10: 95–104.

45. Afifi AH, Shafy HLA, Ramadan AA, Ataa MA, Assad SN. Role of quantitative chemical shift magnetic resonance imaging and chemical shift subtraction technique in discriminating adenomatous from non adenomatous adrenal solid lesions. Egypt J Radiol Nucl Med 2017; 48: 271–284.

46. Israel GM, Korobkin M, Wang C, Hecht EN, Krinsky GA.

Comparison of unenhanced CT and chemical shift MRI in evaluating lipid-rich adrenal adenomas. AJR 2004; 183: 215–219.

47. Fujiyoshi F, Nakajo M, Fukukura Y, Tsuchimochi S. Characterization of adrenal tumors by chemical shift fast low-angle shot MR imaging: comparison of four methods of quantitative evaluation. AJR 2003; 180: 1649–1657.

48. Warda MHA, Shehata SM, Zaiton F. Chemical-shift MRI versus washout CT for characterizing adrenal incidentalomas. J Clin Imaging 2016; 40: 780–787.

49. Seo JM, Park BK, Park SY, Kim CK. Characterization of lipid-poor adrenal adenoma: chemical-shift MRI and washout CT. AJR 2014; 202: 1043–1050.

50. Cicekci M, Onur MR, Aydin AM, Gul Y, Ozkan Y, Akpolat N, Kocakoc E. The role of apparent diffusion coefficient values in differentiation between adrenal masses. J Clin Imaging 2014; 38: 148–153.

51. Becker-Weidman D, Kalb B, Mittal PK, Harri PA, Arif-Tiwari H, Farris AB, Chen Z, Sungjin K, Mrtin DR. Differentiation of lipid-poor adrenal adenomas from non-adenomas with magnetic resonance imaging: utility of dynamic, contrast enhancement and single-shot T2-weighted sequences. Eur J Radiol 2015; 84: 2045–2051.

52. Schieda N, Blaichman JI, Costa AF, Glikstein R, Hurrell C, James M, Maralani PJ, Shabana W, Tang A, Tsampalieros A et al. Gadolinium-based contrast agents in kidney disease: a comprehensive review and clinical practice guideline issued by the Canadian association of radiologists. Can J of Kidney Health Dis 2018; 5: 1-17.

53. Boland GWL, Blake MA, Holalkere NS, Hahn PF. PET/CT for the characterization of adrenal masses in patients with cancer: qualitative versus quantitative accuracy in 150 consecutive patients. AJR 2009; 192: 956–962.

54. Papadakis GZ, Millo C, Stratakis CA. Benign hormone-secreting adenoma within a larger adrenocortical mass showing intensely increased activity on 18F-FDG PET/CT. Endocrine 2016; 54(1): 269–270.

55. Matsumoto S, Hosoya Y, Lefor AK, Haruta H, Ui T, Kurashina K, Saito S, Ashizawa K, Sasaki T, Kitayama et al. A black adrenal adenoma with high FDG uptake on PET/CT scan in a patient with esophageal carcinoma: a case report. Int J Surg Case Rep 2018; 44: 118–121.

56. Sagan D, Zdunek M, Korobowicz E. Primary myelolipoma of the chest wall. Ann Thorac Surg 2009; 88: e39–e41.

57. Karam AR, Nugent W, Falardeau J, Desai D, Khan A, Shankar S. Multifocal extra-adrenal myelolipoma arising in the greater omentum. Radiology Case 2009; 3(11): 20–23.

58. Omdal DG, Baird DE, Burton BS, Goodhue Jr WW, Giddens EM. Myelolipoma of the thoracic spine. AJNR 1997; 18: 977–979.

59. Kumar M, Duerinckx AJ. Bilateral extraadrenal perirenal myelolipomas: an imaging challenge. AJR 2004; 183: 833–836.

60. Ketelsen D, von Weyhern CH, Horger M. Diagnosis of bilateral giant adrenal myelolipoma. J Clin Oncol 2010; 28(33): e678-e679.

61. Chung HM, Luo FJ, Wu TM, Tsai YC. Adrenal myelolipoma with spontaneous hemorrhage. Urol Sci 2010; 21(3): 152–154.

62. Behan M, Martin EC, Muecke EC, Kazam E. Myelolipoma of the adrenal: two cases with ultrasound and CT findings. AJR 1977; 129: 993–996.

63. Lam KY, Lo CY. Adrenal lipomatous tumours: a 30 year clinico-pathological experience at a single institution. J Clin Pathol 2001; 54: 707–712.

64. Campbell MJ, Obasi M, Wu B, Corwin MT, Fananapazir G. The radiographically diagnosed adrenal myelolipoma: what do we really know? Endocrine 2017; 58: 289–294.

65. Amano T, Takemae K, Niikura S, Kouno M, Amano M. Retroperitoneal hemorrhage due to spontaneous rupture of adrenal myelolipoma. Int J Urol 1999; 6: 585–588.

66. Lesbats-Jacquot V, Cucchi JM, Amoretti N, Novellas S, Chevallier P, Bruneton JN. Lipomatous tumors of the adrenals — a report on 18 cases and review of the literature. Clin Imaging 2007; 31: 335–339.

67. Yildiz L, Akpolat I, Erzurumlu K, Aydin O, Kandemir B. Giant adrenal myelolipoma: case report and review of the literature. Pathol Int 2000; 50: 502–504.

68. Musante F, Derchi LE, Zappasodi F, Bazzocchi M, Riviezzo GC, Banderali A, Cicio GR. Myelolipoma of the adrenal gland: sonographic and CT features. AJR 1988; 151: 961-964.

69. Sandoval MAS, Anel-Quimpo J. A giant myelolipoma discovered as an adrenal incidentaloma: radiological, endocrine and pathological evaluation. BMJ Case Rep 2010; doi:10.1136/bcr.05.2010.3005.

70. Slapa RZ, Kasperlik-Zaluska AA, Migda B, Otto M, Jakubowski WS. Application of parametric ultrasound contrast agent perfusion studies for differentiation of hyperplastic adrenal nodules from adenomas — initial study. Eur J Radiol 2015; 84: 1432–1435.

71. Hsu S, Shu K, Lee WC, Cheng YT, Chiang PH. Adrenal myelolipoma: a 10-year single-center experience and literature review. Kaohsiung J Med Sci 2012; 28: 377–382.

72. Littrell LA, Carter JM, Broski SM, Wenger DE. Extra-adrenal myelolipoma and extramedullary hematopoiesis: imaging features of two similar benign fat-containing presacral masses that may mimick liposarcoma. Eur J Radiol 2017; 93: 185–194.

73. Anis-ul-islam M, Qureshi AH, Zaidi SZ. Adrenal myelolipoma in a young male — a rare case scenerio. J Pak Med Assoc 2016; 66(3): 342–344.

74. Hakim A, Rozeik C. Adrenal and extra-adrenal myelolipomas - a comparative case report. Radiology Case 2014; 8(1): 1–12.

75. Rowe SP, Javadi MS, Solnes LB, Fishman EK. Appearance of adrenal myelolipomas on 2-deoxy-2-(18F)fluoro-D-glucose positron emission tomography-computed tomography. World J Nucl Med 2017; 16(4): 271-274.

76. Gemmel F, Bruinsma H, Oomen P, Collins J. PET/CT incidental detection of bilateral adrenal myelolipomas in a patient with a huge maxillary sinus carcinoma. Clin Nucl Med 2010; 35: 132–133.

77. Babic B, Patel D, Aufforth R, Assadipour Y, Sadowski SM< Quezado M, Nilubol N, Prodanov T, Pacak K, Kebebew E. Pediatric patients with pheochromocytoma and paraganglioma should have routine preoperative genetic testing for common susceptibility genes and imaging to detect extra-adrenal and metastatic tumors. Surgery 2017; 161(1): 220–227.

78. Vanderveen KA, THompson SM, Callstrom MR, Young Jr WF, Grant CS, Farley DR, Richards ML, Thompson GB. Biopsy of pheochromocytomas and paragangliomas: potential for disaster. Surgery 2009; 146(6): 1158-1166.

79. Casola G, Nicolet V, van Sonnenberg E, Withers C, Bretagnolle M, Saba RM, Bret PM. Unsuspected pheochromocytoma: risk of blood-presure alterations during percutaneous adrenal biopsy. Radiology 1986; 159(3): 733-735.

80. Blake MA, Kalra MK, Maher MM, Sahani DV, Sweeney AT, Mueller PER, Hahn PF, Boland GW. Pheochromocytoma: an imaging chameleon. RadioGraphics 2004; 24:S87–S99.

81. Park BK, Kim CK, Kwon GY, Kim JH. Re-evaluation of phe-

ochromocytomas on delayed contrast-enhanced CT: washout enhancement and other imaging features. Eur Radiol 2007; 17: 2804–2809.

82. Blake MA, Krishnamoorthy SK, Boland GW, Sweeney AT, Pitman MB, Harisinghani M, Mueller PR, Hahn PF. Low-density pheochromocytoma on CT: a mimicker of adrenal adenoma. AJR 2003; 181: 1663–1668.

83. Patel J, Davenport MS, Cohan RH, Caoili EM. Can established CT attenuation and washout criteria for adrenal adenoma accurately exclude pheochromocytoma? AJR 2013; 201: 122–127.

84. Kim DW, Yoon SK, Kim SH, Kang EJ, Kwon HJ. Assessment of clinical and radiologic differences between small and large adrenal pheochromocytomas. Clin Imag 2017; 43: 153–157.

85. Zhang GMY, Shi B, Sun H, Jin ZY, Xue HD. Differentiating pheochromocytoma from lipid- poor adrenocortical adenoma by CT texture analysis: feasibility study. Abdom Radiol 2017; 42: 2305–2313.

86. Schieda N, Alrashed A, Flood TA, Samji K, Shabana W, McInnes MDF. Comparison of quantitative MRI and CT washout analysis for differentiation of adrenal pheochromocytoma from adrenal adenoma. AJR 2016; 206: 1141–1148.

87. Huang KH, Chung SD, Chen SC, Chueh SC, Pu YS, Lai MK, Lin WC. Clinical and pathological data of 10 malignant pheochromocytomas: long-term follow up in a single institute. Int J Urol 2007; 14: 181–185.

88. Lenders JWM, Duh QY, Eisenhofer G, Gimenez-Roqueplo AP, Grebe SKG, Murad MH, Naruse M, Pacak K, Young Jr WF. Pheochromocytoma and paraganglioma: an endocrine society clinical practice guideline. J Clin Endocrinol Metab 2014; 99(6): 1915–1942.

89. Northcutt BG, Raman SP, Long C, Oshmyansky AR, Siegelman SS, FIshman EK, Johnson PT. MDCT of adrenal masses: can dual-phase enhancement patterns be used to differentiate adenoma and pheochromocytoma? AJR 2013; 201: 834–839.

90. Woo S, Suh CH, Kim SY, Cho JY, Kim SH. Pheochromocytoma as a frequent false-positive in adrenal washout CT: a systematic review and meta-analysis. Eur Radiol 2018; 28: 1027–1036.

91. Timmers HJLM, Chen CC, Carrasquillo JA, Whatley M, Ling A, Eisenhofer G, King KS,Rao JU, Wesley RA, Adams KT et al. Staging and functional characterization of pheochromocytoma and paraganglioma by 18F-fluorodeoxygucose (18F-FDG) positron emission tomography. J Natl Cancer Inst 2012; 104: 700-708.

92. Nakajo M, Nakajo M, Fukurura Y, Jinguji M, Shindo T, Nakabeppu Y, Kamimura K, Yoneyama T, Takumi K, Yoshiura T. Diagnostic performances of FDG-PET/CT and diffusion-weighted imaging indices for differentiating benign pheochromocytoma from other benign adrenal tumors. Abdom Imaging 2015; 40: 1655–1665.

93. Hida T, Nishie A, Asayama Y, Ishigami K, Ushijima Y, Takayama Y, Fujita N, Shimamoto D, Yokomizo A, Tatsugami K et al. Apparent diffusion coefficient characteristics of various adrenal tumors. Magn Reson Med Sci 2014; 13(3): 183–189.

94. Umanodan T, Fukukura Y, Kamagae Y, Shindo T, Nakajo M, Takumi K, Nakajo M, Hakamada H, Umanodan A, Yoshiura T. ADC histogram analysis for adrenal tumor histogram analysis of apparent diffusion coefficient in differentiating adrenal adenoma from pheochromocytoma. J Magn Reson Imaging 2017; 45: 1195–1203.

95. Chang CA, Pattison DA, Tothil RW, Kong G, Akhurst TJ, Hicks RJ, Hofman MS. 68Ga-DOTATATE and 18F-FDG PET/CT in paraganglioma and pheochromocytoma: utility, patterns and heterogeneity. Cancer Imaging 2016; 16(1): 22. doi 10.1186/s40644-016-0084-2.

96. Timmers HJLM, Chen CC, Carrasquillo, Whatley M, Ling A, Havekes B, Eisenhofer G, Martiniova L, Adams KT, Pacak K. Comparison of 18F-fluoro-L-DOPA, 18F-fluoro-deoxyglucose, and 18F-fluorodopamine PET and 123I-MIBG scintigraphy in the localization of pheochromocytoma and paraganglioma. J Clin Endocrinol Metab 2009; 94(12): 4757-4767.

97. Tiwari A, Shah N, Sarathi V, Malhotra G, Bakshi G, Prakash G, Khadilkar K, Pandit R, Lila A, Bandgar T. Genetic status determines 18F-FDG uptake in pheochromocytoma/paraganglioma. J Med Imaging Radiat Oncol 2017; 61: 745–752.

98. Timmers HJLM, Chen CC, Carrasquillo JA, Whatley M, Ling A, Eisenhofer G, King KS, Rao JU, Wesley RA, Adams KT et al. Staging and functional characterization of pheochromocytoma and paraganglioma by 18F-fluorodeoxyglucose (18F-FDG) positron emission tomography. J Natl Cancer Inst 2012; 104: 700-708.

99. Fiebrich HB, Brouwers AH, Kerstens MN, Pijl MEJ, Kema IP, de Jong JR, Jager PL, Elsinga PH, Dierckx RA, van der Wal JE et al. 16-F-18.fluoro-L-dihydroxyphenylalanine positron emission tomography is superior to conventional imaging with 123I-metaiodobenzylguanidine scintigraphy, computer tomography, and magnetic resonance imaging in localizing tumors causing catecholamine excess. J Clin Endocrinol Metab 2009; 94: 3922–3930.

100. Taieb D, Jha A, Guerin C, Pang Y, Adams KT, Chen CC, Romanet P, Roche P, Essamet W, Ling A et al. 18F-FDOPA PET/CT imaging of MAX-related pheochromocytoma. J Clin Endocrinol Metab 2018; 103(4): 1574–1582.

101. Feral CC, Tissot FS, Tosello L, Fakhry N, Sebag F, Pacak K, Taieb D. 18F-fluorodihydroxyphenylalanine PET/CT in pheochromocytoma and paraganglioma: relation to genotype and amino acid transport system L. Eur J Nucl Med Mol Imaging 2017; 44: 812–821.

102. Amodru V, Guerin C, Delcourt S, ROmanet P, Loundou A, Viana B, Bru T, Castinetti F, Sebag F, Pacak K, Taieb et al D. Quantitative 18 F-DOPA PET/CT in pheochromocytoma: the relationship between tumor secretion and its biochemical phenotype. Eur J Nucl Med Mol Imaging 2018; 45: 278–282.

103. Wieneke JA, Thomspon LDR, Heffess CS. Adrenal cortical neoplasms in the pediatric population. Am J Surg Pathol 2003; 27(7): 867–881.

104. Michalkiewicz E, Santrini R, Figueiredo B, Miranda ECM, Caran E, Oliveria-Filho AG, Marques R, Pianovski MAD, Lacerda L, Cristofani LM et al. Clinical and outcome characteristics of children with adrenocortical tumors: a report from the international pediatric adrenocortical tumor registry. J Clin Oncol 2004; 22: 838-845.

105. Gupta N, Rivera M, Novotny P, Rodriguez V, Bancos I, Lteif A. Adrenocortical carcinoma in children: a clinicopathological analysis of 41 patients at the Mayo clinic from 1950 to 2017. Horm Res Paediatr 2018; 90: 8–18.

106. Yadav P, Arora S, Srivastava D, Lal H. Adrenocortical carcinoma with inferior vena cava tumour thrombus: multidetector CT (MDCT) evaluation and management. BMJ Case Rep 2015; doi:10.1136/bcr-2015- 213073.

107. Jiang M, Ding H, Li C, Xiang K, Tang J, Guo Y, Zhang S. Surgical resection of adrenocortical carcinoma with invasion into the inferior vena cava: a case report and literature review. Clinical Case Reports 2017; 5(12): 1934–1937.

108. Hussain S, Belldegrun A, Seltzer SE , Richie JP, Gittes RF, Abrams HL. Differentiation of malignant from benign adrenal Masses: predictive indices on computed tomography. AJR 1985; 144: 61-65.

109. Petersenn S, Richter PA, Broemel T, Ritter CO, Deutschbein

T, Bell FU, Allolio B, Fassnacht M. Computed tomography criteria for discrimination of adrenal adenomas and adrenocortical carcinomas: analysis of the German ACC registry. Eur J Endocrinol 2015; 172(4): 415-422.

110. Fishman EK, Deutch BM, Hartman DS, Goldman SM, Zerhouni EA, Siegelman SS. Primary adrenocortical carcinoma: CT evaluation with clinical correlation. AJR 1987; 148: 531-535.

111. Zhang HM, Perrier ND, Grubbs EG, Sircar K, Ye ZX, Lee JE, Ng CS. CT features and quantification of the characteristics of adrenocortical carcinomas on unenhanced and contrast-enhanced studies. Clin Radiol 2012; 67(1): 38–46.

112. Slattery JMA, Blake MA, Kalra MK, Misdraji J, Sweeney AT, Copeland PM, Mueller PER, Boland GW. Adrenocortical carcinoma: contrast washout characteristics on CT. AJR 2006; 187: W21-W24.

113. Chen L, Zeng X, Li S, Gong C, Peng E, Wu B, Zhang W, Zhang Y. Evaluation of a large adrenal carcinoma with 3D reconstruction of computed tomography images: a case report and literature review. J X-Ray Sci Technol 2016; 24: 665–671.

114. Mitterberger MM, Pinggera GM, Peschel R, Bartsch G, Pallwein L, Frauscher F. The use of three-dimensional computed tomography for assessing patients before laparoscopic adrenal-sparing surgery. BJU Int 2006; 98: 1068-1073.

115. Belmihoub I, Silvera S, Sibony M, Dousset B, Legmann P, Bertagna X, Bertherat J, Assie G. From benign adrenal incidentaloma to adrenocortical carcinoma: an exceptional random event. Eur J Endocrinol 2017; 176: K15-K19.

116. Nogueira TM, Lirov R, Caoili EM, Lerario AM, Miller BS, Fragoso MCBV, DUnnick NR, Hammer GD, Else T. Radiographic characteristics of adrenal masses preceding the diagnosis of adrenocortical cancer. Horm Canc 2015; 6: 176–181.

117. Cistaro A, Asabella AN, Coppolino P, Quartuccio N, Altini C, Cucinotta M, Alongi P, Balma M, Sanfilippo S, Buschiazzo et al. Diagnostic and prognostic value of 18F-FDG PET/CT in comparison with morphological imaging in primary adrenal gland malignancies – a multicenter experience. Hell J Nucl Med 2015; 18(2): 97–102.

118. Hennings J, Lindhe O, Bergstrom M, Langstrom B, Sundin A, Hellman P. 11C.Metomidate positron emission tomography of adrenocortical tumors in correlation with histopathological findings. J Clin Endocrinol Metab 2006; 91: 1410-1414.

119. Minn H, Salonen A, Friberg J, Roivainen A, Viljanen T, Langsjo J, Salmi J, Valimaki M, Nagren K, Nuutila P. Imaging of adrenal incid;entalomas with PET using 11C-metomidate and 18F-FDG. J Nucl Med 2004; 45(6): 972–980.

120. Khan TS, Sundin A, Juhlin C, Langstrom B, Bergstrom M, Eriksson B. 11C-metomidate PET imaging of adrenocortical cancer. Eur J Nucl Med 2003; 30: 403-410.

121. Ardito A, Massaglia C, Pelosi E, Zagiia B, Basile V, Brambilia R, Vigna-Taglianti F, Duregon E, Arena V, Perotti P, Penna D, Terzolo M. 18F-FDG PET/CT in thepost-operative monitoring of patients with adrenocortical carcinoma. Eur J Endocrinol 2015; 173(6): 749-756.

122. Takeuchi S, Balachandran A, Habra MA, Phan AT, Bassett Jr RL, Macapinlac HA, Chuang HH. Impact of 18F-FDG PET/CT on the management of adrenocortical carcinoma: analysis of 106 patients. Eur J Nucl Med Mol Imaging 2014; 41: 2066–2073.

123. Park SY, Park BK, Kim CK. The value of adding 18F-FDG PET/CT to adrenal protocol CT for characterizing adrenal metastasis (≥ 10 mm) in oncologic patients. AJR 2014; 202: W153–W160.

124. Yoo JY, McCoy KL, Carty SE, STang MT, Armstrong MJ, Howell GM, Bartlett DL, Tublin ME, Yip L. Adrenal imaging features predict malignancy better than tumor size. Ann Surg Oncol 2015; 22: S721-S727.

125. Lang BHH, Cowling BJ, Li JYY, Wong KP, Wan KY. High false positivity in positron emission tomography is a potential diagnostic pitfall in patients with suspected adrenal metastasis. World J Surg 2015; 39: 1902–1908.

126. Kim JY, Kim SH, Lee HJ, Kim MJ, Kim YH, Cho SH, Won KS. Utilisation of combined 18F-FDG PET/CT scan for differential diagnosis between benign and malignant adrenal enlargement. Br J Radiol 2013; 86: 20130190.

127. Yasaka K, Gonoi W, Akai H, Kasura M, Akahane M, Kiryu S, Ohtomo K. Differentiation of adrenal tumors in patients with hepatocellular carcinoma: adrenal adenoma versus metastasis. Eur J Radiol 2013; 82: 1213–1218.

128. Hijioka S, Sawaki A, Mizuno N, Hara K, Mekky MA, El-Amin H, Sayed ZEA, Tajika M, Niwa Y, Tamao K. Contrast-enhanced endoscopic ultrasonography (CE-EUS) findings in adrenal metastasis from renal cell carcinoma. J Med Ultrasonics 2011; 38: 89–92.

129. Sasaguri K, Takahashi N, Takeuchi M, Carter RE, Leibovich BC, Kawashima A. Differentiation of benign from metastatic adrenal masses in patients with renl cell carcinoma on contrast-enhanced CT. AJR 2016; 207: 1031–1038.

130. Mouka V, Tsili AC, Messinis T, Papoudou-Bai A, Kamina S, Argyropoulou MI. Solitary adrenal metastasis from early-stage dedifferentiated endometrial carcinoma: CT findings and review of the literature. Journal of Obstetrics and Gynaecology 2016; 36(7); 881-882.

131. Yun M, Kim W, Alnafisi N, Lacorte L, Jang S, Alavi A. 18F-FDG PET in characterizing adrenal lesions detected on CT or MRI. J Nucl Med 2001; 42: 1795–1800.

132. Refaat R, Elghazaly H. Employing 18F-FDG PET/CT for distinguishing benign from metastatic adrenal masses. Egypt J Radiol Nucl Med 2017; 48: 1065–1071.

133. Zhao H, Lin C, Jiao B, Sa R, Hou S, Xu S. Case report of 18F–fluorodeoxyglucose positron emission tomography-computed tomography imaging of a patient with multiple endocrine gland metastases from small cell lung cancer. Thorac Cancer 2018; 9: 167–170.

134. Cho AR, Lim I, Na II, Choe DH, Park JY, Kim BI, Cheon GJ, Choi CW, Lim SM. Evaluation of adrenal masses in lung cancer patients ssing F-18 FDG PET/CT. Nucl Med Mol Imaging 2011; 45: 52–58.

135. Kumar R, Xiu Y, Yu JQ, Takalkar A, El-Haddad G, Potenta S, Kung J, Zhuang H, Alavi A. 18F-FDG PET in evaluation of adrenal lesions in patients with lung cancer. J Nucl Med 2004; 45: 2058–2062.

136. Xie J, Dai J, Zhou WL, Sun FK. Adrenal ganglioneuroma: features and outcomes of 42 cases in a Chinese population. World J Surg 2018; 42: 2469–2475.

137. Lee JH, Chai YJ, Kim TH, Choi JY, Lee KE, Kim HY, Yoon YS, Kim HH. Clinicopathological features of ganglioneuroma originating from the adrenal glands. World J Surg 2016; 40: 2970–2975.

138. Iacobone M, Torresan F, Citton M, Schiavone D, Viel G, Favia G. Adrenal ganglioneuroma: the Padua endocrine surgery unit experience. Int J Surg 2017; 41: S103–S108.

139. Qing Y, Bin X, Jian W, Li G, Linhui W, Bing L, Huiqing W, Yinghao S. Adrenal ganglioneuromas: a 10-year experience in a Chinese population. Surgery 2010; 147: 854–860.

140. Johnson GL, Hruban RH, Marshall FF, Fishman EK. Primary adrenal ganglioneuroma: CT findings in four patients. AJR 1997; 169: 169–171.

141. Otal P, Mezghani S, Hassissene S, Maleux G, Colombier D, Rousseau H, Joffre F. Imaging of retroperitoneal ganglioneuroma. Eur Radiol 2001; 11: 940–945.

142. Shawa H, Elsayes KM, Morani A, Williams MD, Lee JE,

Waguespack SG, Busaidy NL, Vassilopoulou-Sellin R, Jimenez C et al. Adrenal ganglioneuroma: features and outcomes of 27 cases at a referral cancer centre. Clin Endocrinol 2014; 80: 342–347.

143. Sasaki S, Yasuda T, Kaneto H, Otsuki M, Tabuchi Y, Fujita Y, Kubo F, Tsuji M, Fujisawa K, Kasami R et al. Large adrenal ganglioneuroma. Intern Med 2012; 51: 2365–2370.

144. Kamoun M, Mnif MF, Rekik N, Belguith N, Charfi N, Mnif L, Mouna Elleuch, Minf F Kamoun T, Mnif Z et al. Ganglioneuroma of adrenal gland in a patient with Turner syndrome. Ann Diagn Pathol 2010; 14: 133–136.

145. Majbar AM, Elmouhadi S, Elaloui M, Raiss M, Sabbah F, Hrora A, Ahallat M. Imaging features of adrenal ganglioneuroma: a case report. BMC Res Notes 2014; 7: 791.

146. Adas M, Koc B, Adas G, Ozulker F, Aydin T. Ganglioneuroma presenting as an adrenal incidentaloma: a case report. J Med Case Rep 2014; 8: 131.

147. Scherer A, Niehues T, Engelbrecht V, Modder U. Imaging diagnosis of retroperitoneal ganglioneuroma in childhood. Pediatr Radiol 2001; 31: 106–110.

148. Zhang X, Li C, Xu C, Hao X, Yu X, Li Q. Correlation of CT signs with lymphatic metastasis and pathology of neuroblastoma in children. Oncol Lett 2018; 16: 2439–2443.

149. Decarolis B, Simon T, Krug B, Leuschner I, Vokuhl C, Kaatsch P, con Schweinitz D, Klingebiel T, Mueller I, Schweigerer L et al. Treatment and outcome of ganglioneuroma and ganglioneuroblastoma intermixed. BMC Cancer 2016; 16: 542.

150. He WG, Yan Y, Tang W, Cai R, Ren G. Clinical and biological features of neuroblastic tumors: a comparison of neuroblastoma and ganglioneuroblastoma. Oncotarget 2017; 8(23): 37730–37739.

151. Patterson AR, Barker CS, Loukota RA, Spencer J. Ganglioneuroma of the mandible resulting from metastasis of neuroblastoma. Int J Oral Maxillofac Surg 2009; 38: 196–198.

152. Aslan M, Alis D, Kalyoncu AU, Habibi HA, Ozdemir GN, Koc B, Adaletli I. Bilateral cystic adrenal neuroblastoma with cystic liver metastasis. APSP J Case Rep 2017; 8: 1.

153. Mehta SV, Lim-Dunham JE. Ultrasonographic appearance of pediatric abdominal neuroblastoma with inferior vena cava extension. J Ultrasound Med 2003; 22: 1091-1095.

154. Cassady C, Winters WD. Bilateral cystic neuroblastoma: imaging features and differential diagnoses. Pediatr Radiol 1997; 27: 758–759.

155. Chen CP, Chen SH, Chuang CY, Lee HC, Hwu YM, Chang PY, Chen ML, Chen BF. Clinical and perinatal sonogrpahic features of congenital adrenal cystic neuroblastoma: a case report with review of the literature. Ultrasound Obstet Gynecol 1997; 10: 68-73.

156. White SJ, Stuck KJ, Blane CE, Silver TM. Sonography of neuroblastoma. AJR 1963; 141: 465-468.

157. Boyd DT, Hayeri MR, Kadom N. Parotid metastasis from adrenal neuroblastoma. Pediatr Radiol 2010; 40: S113–S115.

158. Werner H, Daltro P, Davaus T, Junior EA. Fetal neuroblastoma: ultrasonography and magnetic resonance imaging findings in the prenatal and postnatal IV-S stage. Obstet Gynecol Sci 2016; 59(5): 407–410.

159. Cohen MD, Weetman R, Provisor A, McGuire W, McKenna S, Smith JA, Carr B, Siddiqui A, Mirkin D, Seo I et al. Magnetic resonance imaging of neuroblastoma with a 0.15-T magnet. AJR 1984; 143: 1241-1248.

160. Leung A, Shapiro B, Hattner R, Kim E, de Kraker J, Ghazzar N, Hartmann O, Hoefnagel CA, Jamadar DA, Kloos R. Specificity of radioiodinated MIBG for neural crest tumors in childhood. J Nucl Med 1997; 38: 1352-1357.

161. Gelfand MJ, Elgazzar AH, Kriss VM, Masters PR, Golsch GJ. Iodine-123-MIBG SPECT versus planar imaging in children with neural crest tumors. J Nucl Med 1994; 35: 1753–1758.

162. Biasotti S, Garaventa A, Villavecchia GP, Cabria M, Nantron M, De Bernardi B. False-negative metaiodobenzylguanidine scintigraphy at diagnosis of neuroblastoma. Med Pediatr Oncol 2000; 35: 153–155.

163. Melzer HI, Coppenrath E, Schmid I, Albert MH, von Schweinitz D, Tudball C, Bartenstein P, Pfluger T. 123I-MIBG scintigraphy/SPECT versus in paediatric neuroblastoma. Eur J Nucl Med Mol Imaging 2011; 38: 1648–1658.

164. Kroiss AS, Uprimny C, Shulkin BL, Gruber L, Frech A, Jazbec T, Girod PP, Url C, Thome C, Riechelmann H et al. 68Ga-DOTATOC PET/CT in the localization of metastatic extra-adrenal paraganglioma and pheochromocytoma compared with 18F-DOPA PET/CT. Rev Esp Med Nucl Imagen Mol 2019; doi: 10.1016/j.remn.2018.09.004.

165. Pfluger T, Schmied C, Porn U, Leinsinger G, Vollmar C, Dresel S, Schmid I, Hahn K. Integrated imaging using MRI and 123I metaiodobenzylguanidine scintigraphy to improve sensitivity and specificity in the diagnosis of pediatric neuroblastoma. AJR 2003; 181: 1115–1124.

166. Zhuang B, Lv DK, Gao SJ, Meng JJ. Differential diagnosis of CT images in children with neuroblastomas and ganglioneuroblastomas. Asian Pac J Cancer Prev 2014; 15(23): 10509–10512.

167. Gahr N, Darge K, Hahn G, Kreher BW, Von Buiren M, Uhl M. Diffusion-weighted MRI for differentiation of neuroblastoma and ganglioneuroblastoma/ganglioneuroma. Eur J Radiol 2011; 79: 443–446.

168. Paling MR, Williamson BRJ. Adrenal involvement in non-Hodgkin lymphoma. AJR 1983; 141: 303–305.

169. Tanpitukpongse TP, Kamalian S, Punsoni M, Gupta M, Katz DS. Radiology–pathology conference: primary adrenal lymphoma. J Clin Imaging 2012; 35: 156–159.

170. Ezer A, Parlakgumus A, Kocer NE, Colakoglu T, Nursal GN, Yildirim S. Primary adrenal non-Hodgkin's lymphoma. Turk J Gastroenterol 2011; 22(6): 643–647.

171. Singh D, Kumar L, Sharma A, Vijayaraghavan M, Thulkar S, Tandon N. Adrenal involvement in non-Hodgkin's lymphoma: four cases and review of literature. Leukemia & Lymphoma 2009; 45(4): 789-794.

172. Pagliuca A, Gillett DS, Salisbury JR, Basu RN, Mufti GJ. Bilateral adrenal lymphoma presenting as Addison's disease. Postgrad Med J 1989; 65: 684–686.

173. Cunningham JJ. Ultrasonic findings in " primary" lymphoma of the adrenal area. J Ultrasound Med 1983; 2: 467-469.

174. Li Y, Sun H, Gao S, Bai R. Primary bilateral adrenal lymphoma: 2 case reports. J Comput Assist Tomogr 2006; 30: 791–793.

175. Joseph FG, Cook S, Gowda D. Primary adrenal lymphoma with initial presentation concerning for bilateral adrenal pheochromocytomas. BMJ Case Rep 2017; doi:10.1136/bcr-2017- 220549.

176. Aravamudan VM, Fong PK, Sam YS, Singh P, Ng SB, Kumar GSP. A rare case of primary bilateral adrenal lymphoma. Case Rep Med 2017; 2017: 1251950.

177. Apter S, Avigdor A, Gayer G, Portnoy O, Zissin R, Hertz M. Calcification in lymphoma occurring before therapy: CT features and clinical correlation. AJR 2002; 178: 935–938.

178. Zhou L, Peng W, Wang C, Liu X, Shen Y, Zhou K. Primary adrenal lymphoma: radiological; pathological, clinical correlation. Eur J Radiol 2012; 81: 401–405.

179. Ekhzaimy A, Mujamammi A. Bilateral primary adrenal lymphoma with adrenal insufficiency. BMJ Case Rep 2016. doi:10.1136/bcr-2016- 217417.

180. Altaiar A, Aslan A, Gunduz N, Alimoglu O, Ayaz E. Unilateral primary adrenal B-cell lymphoma clinically mimicking chronic gastritis. Pol J Radiol 2017; 82: 612–615.

181. Ram N, Rashid O, Farooq S, Ulhaq I, Islam N. Primary adrenal non-Hodgkin lymphoma: a case report and review of the literature. J Med Case Rep 2017; 11: 108.

182. Erdogan G, Gullu S, Colak T, Kamel AN, Baskal N, Ekinci C. Non-Hodgkin's presenting as thyroid and adrenal gland involvement. Endocr J 1997; 44(1): 199–203.

183. Zhou J, Zhao Y, Gou Z. High 18F-fluorodeoxyglucose uptake in primary bilateral adrenal diffuse large B-cell lymphomas with nongerminal center B-cell phenotype. Medicine 2018; 97(17): e0480.

184. Nishiuchi T, Imachi H, Fujiwara M, Muaro K, Onishi H, Kiguchi T, Takimoto H, Kushida Y, Haba R, Ishida T. A case of non-Hodgkin's lymphoma primary arising in both adrenal glands associated with adrenal failure. Endocr 2009; 35: 34-37.

185. Martinez-Esteve A, Garcia-Gomez FJ, Madrigal-Toscano MD, Borrego-Dorado I. Primary bilateral diffuse large B-cell lymphoma of the adrenals. Br J Haematol 2015; 170(1): 3.

186. Forbes TL. Retroperitoneal hemorrhage secondary to a ruptured cavernous hemangioma. J Can Chir 2005; 48(1): 78.

187. Oh BR, Jeong YY, Ryu SB, Park YI, Kang HK. A case of adrenal cavernous hemangioma. Int J Urol 1997; 4: 608–610.

188. Marotti M, Sucic Z, Krolo I, Dimanovski J, Klaric R, Ferencic Z, Karapanda N, Babic N, Pavlekovic K. Adrenal cavernous hemangioma: MRI, CT, and US appearance. Eur Radiol 1997; 7: 691–694.

189. Xu HX, Liu GJ. Huge cavernous hemangioma of the adrenal gland. J Ultrasound Med 2003; 22: 523-526.

190. Feo CV, De Troia A, Pedriali M, Sala S, Zatelli MC, Carcoforo P, Feo CF. Adrenal cavernous hemangioma: a case report. BMC Surg 2018; 18(1): 103.

191. Zemni I, Haddad S, Hlali A, Manai MH, Essoussi. Adrenal gland hemangioma: a rare case of the incidentaloma: case report. Int J Surg Case Rep 2017; 41: 417–422.

192. Agrusa A, Romano G, Salamone G, Orlando E, Di Buono G, Chianetta D, Sorce V, Gulotta L, Galia M, Gulotta G. Large cavernous hemangioma of the adrenal gland: laparoscopic treatment. Report of a case. Int J Surg Case Rep 2015; 16: 150–153.

193. Arkadopoulos N, Kyriazi M, Yiallourou AI, Stafyla VK, Theodosopoulos T, Dafnios N, Smyrniotis V, Kondi-Pafiti A. A rare coexistence of adrenal cavernous hemangioma with extramedullar hemopoietic tissue: a case report and brief review of the literature. World J Surg Oncol 2009; 7: 13.

194. Thiele JW, Bodie B. Adrenal hemangioma. Surgery 2001; 129: 373-374.

195. Telem TA, Nguyen SQ, Chin EH, Weber K, Divino CM. Laparoscopic resection of giant adrenal cavernous hemangioma. JSLS 2009; 13: 260–262.

196. Heis HA, Bani-Hani KE, Bani-Hani BK. Adrenal cavernous haemangioma. Singapore Med J 2008; 49(9): e236-e237.

197. Quildrian SD, SIlberman EA, Vigovich FA, Porto EA. Giant cavernous hemangioma of the adrenal gland. Int J Surg Case Rep 2013; 4: 219–221.

198. Matsuda D, Iwamura M, Baba S. Cavernous hemangioma of the adrenal gland. Int J Urol 2009; 16: 424.

199. Ellis CL, Banerjee P, Carney E, Sharma R, Netto GJ. Adrenal lymphangioma: clinicopathologic and immunohistochemical characteristics of a rare lesion. Hum Pathol 2011; 42: 1013–1018.

200. Lin TP, Chen M, Chen CK, Hsu JM, Lin WR. Adrenal cystic lymphangioma: a case report and review of the literature. Urol Sci 2014; 25: 112–114.

201. Liu B, Li Y, Wang S. Adrenal lymphangioma removed by a retroperitoneoscopic procedure. Oncol Lett 2013; 5: 539–540.

202. Secil M, Demir O, Yorukoglu K. MRI of adrenal lymphangioma: a case report. Quant Imaging Med Surg 2013; 3(6): 347–348.

203. Bibi M, Sellami A, Taktak T, Chelly B, Ghorbel Z, Zouari H, Boukriba S, Boussafa H, Chehida MAB, Rhouma SB et al. Giant cystic lymphangioma of adrenal gland: a case report and review of the literature. Urol Case Reports 2019; 22: 6–7.

204. Rowe SP, Bishop JA, Prescott JD, Salvatori R, Fishman EK. CT appearance of adrenal cystic lymphangioma: radiologic-pathologic correlation. AJR 2016; 206: 81–85.

205. Zhao M, Gu Q, Li C, Yu J, Qi H. Cystic lymphangioma of adrenal gland: a clinicopathological study of 3 cases and review of literature. Int J Exp Pathol 2014; 7(8): 5051–5056.

206. Zemheri E, Yildirim A, Ozkanli S, Zenginkinet T, Caskurlu T. Cystic lymphangioma of the adrenal gland: case report. World J Nephrol Urol 2013; 2(2): 82–84.

207. Jung HI, Ahn T, Son MW, Kim Z, Bae SH, Lee MS, Kim CH, Cho HD. Adrenal lymphangioma masquerading as a pancreatic tail cyst. World J Gastroenterol 2014; 20(36): 13195–13199.

208. Cakir E, Aydin E, Samdanci E, Ates M, Elmali C, Sayin S, Erdem G. Cystic adrenal lymphangioma — report of two cases and review of the literature. J Park Med Assoc 2012; 62(9): 962-964.

209. Jakowski JD, Wakely Jr PE, Jimenez RE. An uncommon type of adrenal incidentaloma: a case report of a schwannoma of the adrenal medulla with cytological, histological, and ultrastructural correlation. Ann Diagn Pathol 2008; 12: 356–361.

210. Hsiao HL, Lin HC, Yeh HC, Huang CH, Wu WJ. Adrenal schwannoma treated with laparoscopic adrenalectomy: a case report. Kaohsiung J Med Sci 2008; 24: 553–557.

211. Suzuki K, Nakanishi A, Kurosaki Y, Nogaki J, Takaba E. Adrenal schwannoma: CT and MRI findings. Radiat Med 2007; 25: 299–302.

212. Xiao C, Xu B, Ye H, Yang Q, Wang L, Sun YH. Experience with adrenal schwannoma in a Chinese population of six patients. J Endocrinol Invet 2011; 34: 417–421.

213. Tarcoveanu E, Dimofte G, Bradea C, Moldovanu R, Vasilescu A, Anton R, Ferariu D. Adrenal schwannoma. SJLS 2009; 13: 116–119.

214. Zhang YM, Lei PF, Chen MN, Lv XF, Ling YH, Cai PQ, Gao JM. CT findings of adrenal schwannoma. Clin Radiol 2016; 71: 464–470.

215. Liu QY, Gao M, Li HG, Lin XF, Huang SQ, Liang BL. Juxta-adrenal schwannoma: dynamic multi-slice CT and MRI findings. Eur J Radiol 2012; 81: 794–799.

216. Hou J, Zhang L, Guo Y, Chen H, Wang W. Primary adrenal schwannoma with catecholamine hypersecretion. Arch Med Sci 2016; 12(3): 681-683.

217. Tang W, Yu XR, Zhou LP, Gao HB, Wang QF, Peng WJ. Adrenal schwannoma: Ct, MR manfestations and pathological correlation. Clin Hemorheol Microcirc 2018; 68(4): 401-412.

218. Yang CY, Chou CW, Lin MB, Li CF. Schwannomas of the left adrenal gland and posterior mediastinum. J Chin Med Assoc 2009; 72(2): 83-87.

219. Onoda N, Ishikawa T, Toyokawa T, Takashima T, Wakasa K, Hirakawa K. Adrenal schwannoma treated with laparoscopic surgery. JSLS 2008; 12: 420–425.

220. Kim SH, Choi BI, Han MC, Kim YI. Retroperitoneal neurilemoma: CT and MR findings. AJR 1992; 159: 1023-1026.

221. Korets R, Berkenblit R, Ghavamian R. Incidentally discovered adrenal schwannoma. JSLS 2007; 11: 113–115.

222. Adas M, Ozulker F, Adas G, Koc B, Ozulker T, Sahin IM. A rare adrenal incidentaloma: adrenal schwannoma. Case Rep Gastroenterol 2013; 7: 420–427.